Universitat Politècnica de Catalunya

Doctoral Thesis

Experimental and numerical study of the symbolic dynamics of modulated semiconductor lasers with optical feedback

Author:

Taciano Amaral Sorrentino

Supervisors:

Prof. Cristina Masoller

Prof. M. Carme Torrent

A thesis submitted in fulfillment of the requirements

for the degree of Doctor in Physics

in the

Research Group on Nonlinear Dynamics, Nonlinear Optics and Lasers

(DONLL)

Departament de Física i Enginyeria Nuclear

To my parents, Aroaldo and Marlene,
to my wife, Patricia.

Contents

Abstract

The goal of this thesis is to investigate the influence of current modulation in the dynamics of the low-frequency fluctuations (LFF) regime induced by optical feedback in semiconductor lasers. In this regime the laser output exhibits apparently random and sudden dropouts that, in some statistical properties, are similar to excitable neuronal spikes. Long time series containing tens of thousands of LFF dropouts were experimentally acquired and simulated, using the Lang and Kobayashi model, under different conditions. By detecting the individual dropouts, the intensity time series were transformed in series of inter-spike intervals (ISI). We then analyzed the ISI sequences by using a symbolic method of analysis capable of unveil serial correlations in data sets, known as ordinal symbolic analysis. Our findings reveal the existence of a hierarchical and clustered organization of ordinal patterns in the ISI series.

When the laser is subject to periodical external forcing, through modulation of the injection current, we identify clear changes in the dynamics as the increase of the modulation amplitude induces deterministic-like behavior in the system. When the modulation frequency is varied, the change in the statistics of the various symbols is empirically shown to be related to specific changes in the ISI distribution, which arise due to different noisy phase-locking regimes.

We also investigated how the spike rate is affected by the modulation, for different parameters that determine the natural (without modulation) spike rate. When the intrinsic spike dynamics is slow, fast modulation can produce faster spikes. When the intrinsic dynamics is already fast, modulation cannot induce much faster spikes. Similar effects were observed in the spike correlations: we found that higher natural spike rates wash out the effects of the modulation in the spike correlations. Simulations of the Lang and Kobayashi model are shown to be in good agreement with the experimental observations.

The results reported in this thesis may be important to the use of semiconductor lasers as optical spiking neurons in information processing networks inspired by biological ones, and more generally, to the analysis of serial correlations in spiking excitable systems. Future

work may include investigations of how correlations that encode an external signal spread in a small network of semiconductor lasers.

Resumen

El objetivo de esta tesis es investigar la influencia de la modulación de corriente sobre la dinámica de los láseres semiconductores con realimentación óptica en el regimen de fluctuaciones de baja frequencia (*low-frequency fluctuations*, o LFF) . En este regimen la intensidad de la salida del láser muestra caídas abruptas y aparentemente aleatorias que son similares, en algunas propiedades estadísticas, a los spikes neuronales excitables. Largas series temporales, que contienen decenas de estas caídas, fuerón adquiridas experimentalmente y simuladas usando el modelo de Lang y Kobayashi, bajo diferentes condiciones. Al detectar las caídas individuales, las series temporales son transformadas en series de intervalos entre caídas (*inter-spike intervals*, o ISI). Seguidamente, se analizan las secuencias de ISI mediante el uso de un método de análisis simbólico, conocidos como análisis simbólico ordinal, capaz de revelar correlaciones seriales en los conjuntos de datos. Nuestros resultados revelan la existencia de una organización jerárquica y agrupada de los patrones ordinales en las series de ISI.

Cuando el láser está sujeto a forzamiento externo periódico, a través de la modulación de la corriente de inyección, identificamos cambios claros en la dinámica. El aumento de la amplitud de modulación induce comportamiento determinista en el sistema. Cuando la frecuencia de modulación es variada, se muestra empíricamente el cambio en las estadísticas de los distintos símbolos, que está relacionado a los cambios específicos en la distribución de los ISI. Estos cambios surgen debido a diferentes regímenes ruidosos en el bloqueo en fase.

También se investigó cómo la frecuencia de aparicion de las caídas se ve afectada por la modulación, para los diferentes parámetros que determinan la frecuencia natural (sin modulación) de las caídas. Cuando la dinámica intrínseca de las caídas es lenta, la modulación rápida puede producir caídas más rápidas. Cuando la intrínseca dinámica ya es rápida, la modulación no puede inducir caídas mucho más rápidas. Efectos similares fueron observados en las correlaciones de las caídas: encontramos que mayores tasas de las caídas nat-

urales acaban con los efectos de la modulación en las correlaciones. Las simulaciones de lo modelo de Lang y Kobayashi se muestran estar en buen acuerdo con las observaciones experimentales.

Los resultados presentados en esta tesis pueden ser importantes para el uso de láseres semiconductores por ejemplo como neuronas ópticas en redes de procesamiento de información, inspiradas en las redes de neuronas biológicas, y más generalmente, para el análisis de las correlaciones seriales en sistemas excitables. El trabajo futuro podría incluir la investigación de cómo correlaciones que codifican una señal externa se propagan en una pequeña red de láseres semiconductores.

Acknowledgements

This work would not be possible without the help of many people.

Firstly I want to thank Prof. Cristina Masoller. For proposing me this work, for her patience (many times challenged in the last years), for all her support and the precious time she invested in me, and for not giving up on me. I also thank very much Prof. Carme Torrent for all her help, her propositions and her care with everything. To Prof. Marcos Oriá and Prof. Martine Chevrollier, from the Universidade Federal da Paraíba in João Pessoa, for the nice three months stay in 2011 and for the support of all times.

I could not be in Catalonia without the help of many people in my home institution, UFERSA. I want to thank my colleages at DCEN, specially the ones that assumed my class duties right after my license: Prof. Júlio César Pereira Barbosa, Prof. Geovani Ferreira Barbosa, Prof. José Luiz Sousa Lima and Prof. Francisco Odolberto de Araújo, former DCEN director and vice-rector. I also wish to thank present DCEN director Prof. Rafael Castelo and former DCEN director Prof. Judson Santiago.

I wish to thank Andrés Aragoneses for his help, kindness and support while we worked together in the lab and to Carlos Quintero for the nice automatization of the experiment, for his help in all kind of computer-related problems and for his friendship during the last year and a half. Jordi Zamora, thanks for your gentleness and your nice programming lessons. José Aparicio Reinoso (Pepe), thanks for your friendship and nice discussions. Ignacio Deza thanks for being a good friend and for supporting me when I had to talk in Madrid to a hall full of Germans, and Spaniards ("so, you are Brazilian..."), in the day after the catastrophic semi-final of the FIFA world cup :)

I'm grateful to all the people from the DONLL group. Prof. Ramón Vilaseca, Prof. Kestas Staliunas, Prof. José Trull, Prof. Ramon Herrero, Dr. Simone Pigolotti, Prof. Toni Pons, Prof.

Crina Cojocaru, Dr. Laura Carpi, Prof. Carles Serrat, Prof. Muriel Botey, Prof. Josep Lluís Font, and Prof. Jordi García Ojalvo. Thank you for the talks and the always nice labmeetings. Thanks also to Montse Gea and to Cristina Fernández for their help.

To Alicia Sanchez and Ana Ortega at the PhD program office, for their help and availability.

To to students and former students of the group, and from UPC, for their good companionship: Andrés, Carlos, Ignacio, Giulio, Sandro, Shubham, Dani, Dario, Lina, Ricard, John, Bingxia, Yu Chieh, Auro, Waqas, Petya, Heather, Belén, Marta, Houssam, Nikhil, Lara, Jordi Tiana and Jordi Zamora.

Obrigado a todos meus fiéis amigos, com quem sempre pude contar, mesmo à distância: Renato, Allan, Aluízio, Tássio, Seigi, Kemyson, César Augusto, Cirilo, Mário César, Valdeci, Weliton.

Obrigado a minha família pelo apoio de todas horas. Pai devo tudo a você, nunca poderei agradecer o suficiente. Mãe, muito obrigado por tudo. Socorro, muito obrigado também. Tati e Tiago, sempre penso em vocês. Gabriel, Cecília e Pedro Henrique, que o tempo lhes reserve sempre coisas boas. Tia Fátima, Gianna e Fabrício, Killiam, seria muito bom sempre tê-los perto.

Patricia, a partir de agora estaremos sempre juntos em nossos aniversários. Oxalá eles demorem muito, sintamos o tempo passar devagar, e que ao final ainda achemos que uma longa vida inteira foi muito pouco. Obrigado por ser quem é. Obrigado por tudo. Amo muito você.

Thank you for reading this work, no matter the reasons why. I hope you find it interesting and that it can be useful to you.

Chapter

1

Introduction

In this first introductory chapter we review concepts about semiconductor lasers and their dynamics necessary for understanding the results presented in this thesis. Semiconductor lasers basics are addressed in section 1.1. Section 1.2 presents general aspects of the dynamics of semiconductor lasers subject to optical feedback. In section 1.3 we focus on the particular remarkable regime induced by optical feedback that we will analyze in this thesis, the low-frequency fluctuations. Section 1.4 presents the main tool of time-series analysis employed in this thesis, ordinal symbolic analysis.

1.1 Semiconductor Lasers

1.1.1 Historical Background

The familiar word 'laser' is an acronym. It stands for "**l**ight **a**mplification by **s**timulated **e**mission of **r**adiation". The physical mechanism of stimulated emission was proposed by Einstein in 1917 [1], and, before the laser, it was exploited in another device, the maser (**m**icrowave **a**mplification by **s**timulated **e**mission of **r**adiation), for which theoretical description was presented by Basov and Prokhorov in 1952, and published in 1954 [2]. The first operational maser was build by Gordon, Zeiger and Townes still in 1954 [3] and the working principles of the laser were proposed in a seminal theoretical paper by Schawlow and Townes in 1958 [4].

Before the experimental realization of the laser it was already recognized that such device would represent a major scientific and technological breakthrough. In 1960 T. H. Maiman [5]

build the first laser, a pulsed rubi laser. This laser was called an optical maser, becoming the word laser more often used only after 1965. Continuous wave operation was achieved just one year after Maiman's device, by Javan *et al.* [6] with a He-Ne gas laser, soon followed by continuous operation of three solid state devices [7–9]. The two years that followed the first rubi laser saw an intense and fruitful search for novel laser media.

The possibility of achieving stimulated emission in semiconductors by the recombination of carriers injected in a p-n junction was first suggested by Basov *et al.* in 1961 [10]. A p-n junction is formed when a type p semiconductor and a type n semiconductor are put in contact. In the following year three laboratories, independently, produced the first semiconductor lasers [11–14]. The performance of those first devices was limited to pulsed operation under cryogenic temperatures. This would change in 1969 with the implementation of the suggestion, already made in 1963 [15], that one layer of semiconductor material should be inserted between two layers of another semiconductor material with larger bandgap, to form an heterostructure laser [16–18].

The progress after 1962 was slower because of a few reasons. The main one is that a new semiconductor technology was necessary, given that it was not possible to make semiconductor lasers from silicon, material for which a developed manufacture technology already existed. The lasers required direct bandgap materials, and composite semiconductors were not so well understood by the time. The introduction of heterostructures by the end of the decade of 1960 decreased significantly the threshold currents and improved the confinement both of photons and carriers in the gain region, allowing the continuous wave operation at room temperature in 1970 [19, 20].

There were two factors that mainly contributed to the transformation from laboratory devices operating at cryogenic temperatures into practical continuous wave, room temperature, optoelectronic devices [21]. The first one was the amazing lattice matching between $AlAs$ and $GaAs$, that allowed heterostructures formed by layers made with different compositions of $Al_xGa_{1-x}As$ to be grown. The second was the vast number of optoelectronic applications for which semiconductor lasers were uniquely appropriate, for being the smallest, the most efficient and the ones with longest lifetime among all existing lasers of the time. These characteristics and the potential for applications have drawn to the field of semiconductor lasers the resources necessary to their development.

Among the applications that most motivated research in semiconductor lasers there is fiber optical communications, for which the fact that one can modulate optical power by modulating the injection current is particularly advantageous. $InGaAsP/InP$ lasers emitting at 1.3 μm, where absorption in silica fibers is minimum, and at 1.55 μm, where dispersion in the fibers is minimum, were obtained in the decade of 1970. Laser amplifiers had to be developed to address the demand for repeaters, the use of underwater communication lines led to improvement on the reliability of the devices and frequency multiplexing led to novel laser designs for frequency stability.

Other applications where also important in semiconductor lasers development. Optical memory applications (audio and data discs) have generated a large demand that helped in reducing laser cost. Other important applications of semiconductor lasers include: high power lasers for welding and cutting in industry; diverse devices in consumer electronics; laser detection and ranging (LIDAR) and gas tracing; medical and dentistry applications in diagnostics and therapy; military and safety systems applications.

1.1.2 Edge-Emitting Semiconductor Lasers

Lasers, in general, are constituted by: a gain medium where the stimulated emissions take place so the incident radiation is amplified; an external energy source that produce and maintain the population inversion in the gain medium (pumping), so stimulated emission can occur in a rate high enough to overcome all the possible losses in the system; and an oscillation cavity that provides optical feedback and confines electromagnetic radiation in well defined modes. What defines a semiconductor laser is the use of a semiconductor material as gain medium.

Semiconductor laser designs can be classified by different criteria: pumping mechanism, the direction of propagation of the amplified optical field relative to the plane of the p-n junction, mechanisms for confining photons and carriers in the active region, cavity design, etc. Here we will review some properties of the type of semiconductor laser used in the experiments reported in this thesis: the edge-emitting diode laser with Fabry-Perot cavity.

A diode laser, or injection laser, is a semiconductor laser for which the excitation of the gain medium is obtained by injecting electric current through the p-n junction. Although this is by far the most used method of excitation, to the point that semiconductor laser in general means diode laser, various other methods have been demonstrated [22].

Edge-emitting refers to the fact that light is emitted through the edges of the laser structure: the optical axis is parallel to the plane of the p-n junction (see Fig. 1.1). In contrast, VCSELs (Vertical Cavity Surface Emitting Lasers) are semiconductor lasers where the light being amplified propagate perpendicular to the junction plane, allowing for a great reduction of the size of the active layer and the size of the laser cavity.

There are three main types of cavity for edge-emitting lasers. A Fabry-Pérot (FP) resonant cavity simply consists in two cleaved end facets. Distributed feedbacks (DFBs) have a periodic structure in the active region, and distributed Bragg reflectors (DBRs) a grating in the refractive index outside the active region. DFB and DBR structures select a single longitudinal mode with a frequency directly related with the periodicity of the structure.

In what follows we describe the type of semiconductor laser used in our experiments, the FP edge-emitting diode laser.

Physical Structure

The essence of a diode laser is its p-n junction. If a diode laser has a p-n junction formed by the same semiconductor, it is called a homostructure laser. If two semiconductors are used in the diode, we have a heterostructure laser. In general a heterostructure laser has in the active region a certain doped semiconductor inserted between two layers of a different semiconductor with larger bandgap and smaller refraction index, one of the layers p-doped and another n-doped. This is a double heterostructure diode laser (see Fig. 1.1). The bandgap difference between the different semiconductors create energy barriers at the junction interfaces, and these energy barriers confine the carriers in the active region (Fig. 1.2a). The difference in the refraction index confine the optical mode in the active region, acting as a dielectric waveguide (Fig. 1.2b). As discussed before, the better confinement of photons and carriers provided by double heterostructures allowed to significant decrease of threshold currents that permitted continuous wave, room temperature operation in 1970 [19, 20].

In the diode laser schematically shown in Fig. 1.1 the lateral confinement of the carriers is due to a stripe-like contact in the central region, that limits the region where the current is conducted and, therefore, the gain region in the junction. This technique is called gain confinement. In this scheme, the optical mode is easily confined by the lateral variation of the optical gain to a region near the electric pumping stripe. Lasers with this kind of lateral

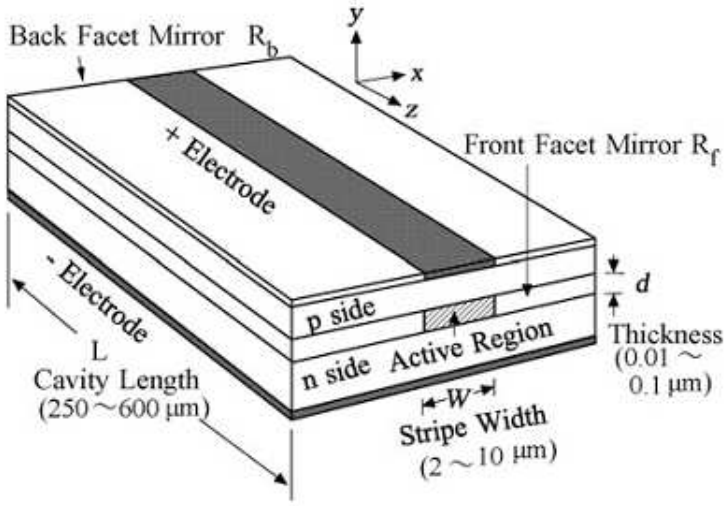

Figure 1.1: Double heteroestructure edge-emitting diode laser. From [23].

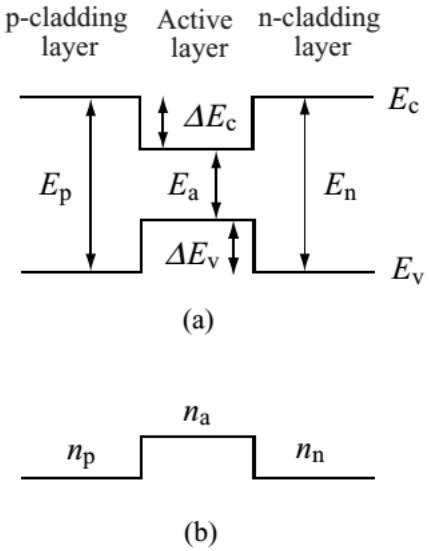

Figure 1.2: Double heteroestructure: (a) energy of carriers. E_c, E_v: conduction and valence band energy levels, respectively; $\Delta E_c, \Delta E_v$: energy barriers for the holes at the interface of the n-cladding layer and the active layer, and energy barrier for the electrons at the interface of the p-cladding layer and the active layer, respectively. (b) Light is confined in the active region due to the differences of refractive index. From [24].

confinement are called gain guided. The lateral confinement of the optical mode in the gain region can also be obtained by lateral variations of the refraction index, and lasers that use this kind of confinement are called index guided lasers.

If a laser has an active layer of thickness much larger than the de Broglie wavelength of

the electron, for example, around 0.1 μm, carriers can be treated as classical particles. If the thickness is reduced to about 10 nm, or less, the quantum nature of the carriers as matter waves appears significantly. The active layer and the surrounding layers form then a narrow potential well where electrons and holes are confined. These lasers are called quantum well lasers. Because of the strong confinement there is an increase in the effective band-gap energy and a modification of the density-of-states function to a step-like function, and consequently, a gain spectrum and polarization dependence different from those of ordinary heterostructures appear [25, 26]. By appropriate design of quantum wells and optimization of waveguide structure, remarkable developments were achieved in the extension of the lasing wavelength region, reduction of the threshold current, enhancement of modulation bandwidth, noise reduction and improvement of spectral purity.

Operation Principles

In the active layer of a diode laser stimulated recombination of electrons whose energies are in the bottom of the conduction band and holes whose energies are in the top of the valence band takes place. When the p-n junction is formed, the quasi-Fermi levels of n- an p-doped semiconductors are not immediately equal because they are in non-equilibrium. The electrons in the n side diffuse to the p side, and the opposite occur for the holes. The diffusing electrons and hole recombine in the junction region. After a steady state is reached, the Fermi level is continuous across the p-n junction as shown in Fig. 1.3a.

When a forward bias is applied through the p-n junction by an external voltage, the built-in electric field is reduced, making possible a further diffusion of electrons and holes across the junction, as shown in Fig. 1.3b. In a narrow depletion region electrons and holes are present simultaneously and can recombine, radiatively or not. For radiative recombination, photons of energy $h\nu \approx E_g$ are emitted, being E_g the energy of the gap between conduction and valence bands. Those photons, however, can be also re-absorbed in an inverse process, generating electron-hole pairs. When the external voltage exceeds a critical value the population inversion is reached and the emission rate of photons overcomes the absorption rate. The p-n junction is able to amplify electromagnetic radiation, for wavelengths such that $\lambda \approx hc/E_g$, and exhibits optical gain.

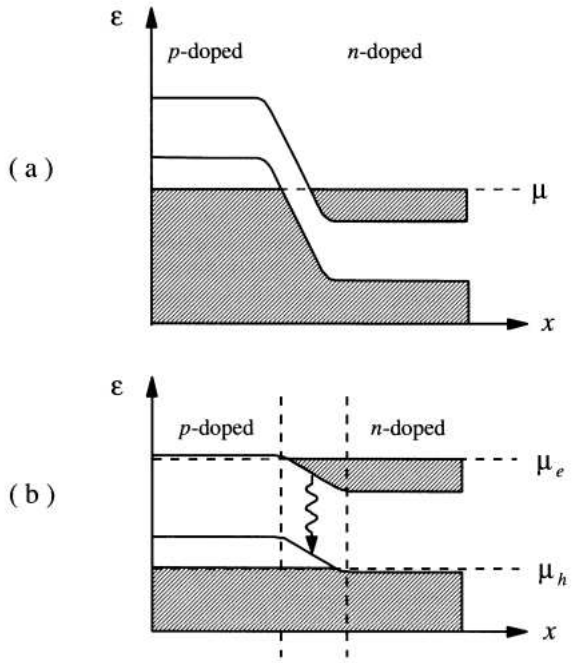

Figure 1.3: Electron energy and occupation perpendicular to the p-n junction. (a) Without an applied voltage. (b) With a forward biased applied voltage. μ, constant Fermi level across the junction in equilibrium. μ_e, Fermi level for electrons, μ_h Fermi level for holes. From [21].

Fabry-Pérot Cavity and Beam Characteristics

As mentioned before, the lasers used in this thesis have Fabry-Pérot (FP) cavities formed by the cleaved facets of the semiconductor crystal. As a semiconductor material has a high refractive index for the emitted wavelengths ($n \approx 3.5$), a cleaved facet in air has a typical reflectivity in the range 25%–35%. This reflectivity is low if compared with mirrors used in other lasers, but due to the high gain in the semiconductor material it is not an issue. FP lasers emit equally from both ends, but they are commonly used with a total-reflection coating in one of the facets, so the total laser power is emitted from the uncoated facet. Lasers with FP cavities (usually referred to as edge-emitting lasers, EELs) typically emit in multiple longitudinal modes with mode spacing given by:

$$\Delta\nu = \frac{c}{2n_g L}, \tag{1.1}$$

where n_g is the group refracting index for the emitted frequency, L is the cavity lenght and c is the speed of light. The predominant mode is the one for which the gain is larger. The

gain curve is given by the energy gap of the semiconductor material. Besides the longitudinal modes, there are also the transversal/lateral modes. Usually the optical confinement is such that the cavity supports only one transversal/lateral mode.

Because the lateral area has small dimensions as compared with the longitudinal ones, the output beam of an edge-emitting laser diode diverges strongly in both directions, but with different angles. A lens of small focal length is generally used to collimate the output beam.

Rate Equations

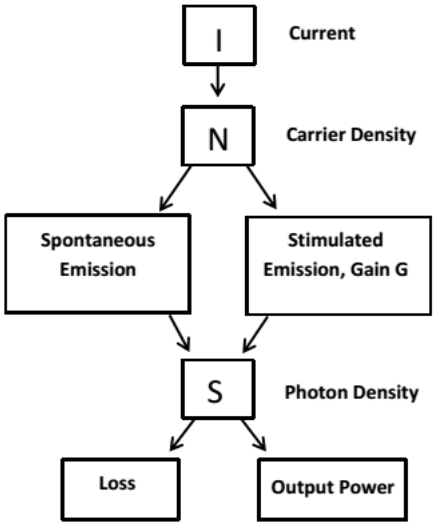

Figure 1.4: Schematic representation of a diode laser. Adapted from [27].

Figure 1.4 schematically illustrates the input-output behavior of a diode laser. A current I flows into the active region. The supplied carriers recombine spontaneously or produce optical gain by stimulated recombination. As a consequence, there is a photon density in the active region. Some of the photons are lost, and some are emitted by the laser and this gives the optical output power.

Considering the diagram above and the balance between current, carrier density and photon density, two phenomenological rate equations that govern the time dependence of the carrier density and the photon density can be written [28]. First, we treat the equation for the carrier density. The carriers are supplied by a current I into the volume of the active

region V. Some of the carriers recombine spontaneously, with a life-time τ_N. Others carriers recombine by stimulated recombination, described by the gain factor G and the photon density, S. The temporal dependence of the carrier density N is then given by

$$\frac{dN}{dt} = \frac{I}{qV} - GS - \frac{N}{\tau_N}. \tag{1.2}$$

At the moment we assume a linear net gain per unit time $G(N) = a(N - N_0)$, being a the differential gain factor and N_0 the transparency value of the carrier density. The temporal dependence of the photon density is described by

$$\frac{dS}{dt} = GS - \frac{S}{\tau_p} + \beta_{sp}\frac{N}{\tau_N}. \tag{1.3}$$

In the right side of equation 1.3 the first term refers to the stimulated recombination. For each stimulated recombination there is one more photon in the active region, and this is the same term that appears in the rate equation for the carrier density with opposite sign. Same photons are lost, and this is described by the photon life-time τ_p. The last term refers to the spontaneous emission. A fraction β_{sp} of all spontaneous recombinations supply one photon to the oscillating mode. Equations 1.2 and 1.3 constitute a set of nonlinear, coupled differential equations.

Re-defining S and N as adimensional variables, equations 1.2 and 1.3 can be re-written in a normalized form, useful when doing simulations:

$$\frac{dN}{dt} = \frac{1}{\tau_N}(I - N - NS) \tag{1.4}$$

$$\frac{dS}{dt} = \frac{1}{\tau_p}(N-1)S + \beta_{sp}. \tag{1.5}$$

Despite their simplicity, neglecting gain-saturation effects and other sources of nonlinearity, the above rate equations are able to reproduce many general characteristics of the dynamics of semiconductor lasers.

Relaxation Oscillations

Because the carrier density increases at a finite rate when the laser is turned on, a delay in the steady operation of the laser is unavoidable. The nonlinear coupling between photons and carriers results in transient oscillations referred to as relaxation oscillations (RO) [28], that play important role in diode lasers dynamics.

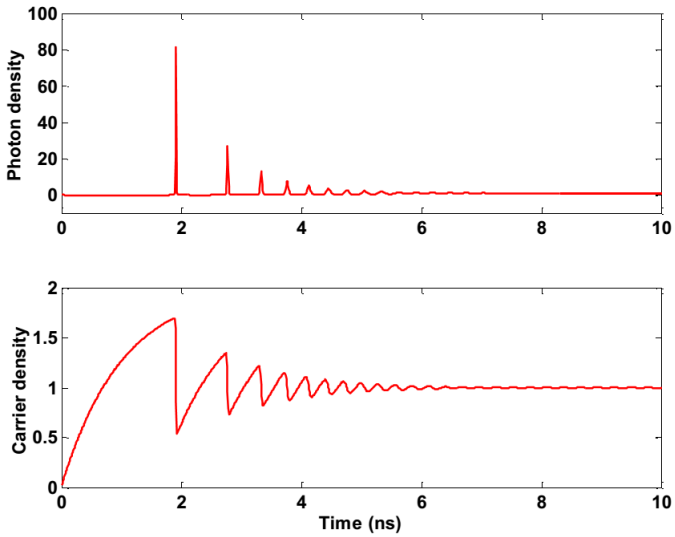

Figure 1.5: Relaxation oscillations that follow a diode laser turning on, obtained by integration of equations 1.5 and 1.4. $\tau_p = 1$ ps, $\tau_N = 1$ ns, $I = 2$, $\beta_{sp} = 10^{-5}$.

Figure 1.5 shows the behavior of photon density and carrier density when equations 1.5 and 1.4 are integrated over 10 nanoseconds. The frequency of the oscillations can be shown to depend only of the injection current and photon and carrier lifetimes [28]:

$$f_r = \frac{1}{2\pi}\sqrt{\frac{I-1}{\tau_p \tau_N}}. \tag{1.6}$$

As typical values of τ_p and τ_N are around 10^{-12} s and 10^{-9} s, respectively, f_r values are about a few GHz, depending on I.

Light-Current Characteristics

As the injection current is increased more carriers are available in the active region for stimulated recombination. The current for which the radiation gain due to stimulated emission

equal losses is called threshold current (I_{th}). For $I < I_{th}$ the output power is mainly due to spontaneous emission, as shown in Fig. 1.6. For $I > I_{th}$ the output power increases linearly with the injection current as $P_{out} = \eta_D(I - I_{th})$, being η_D the differential efficiency of the laser. The shape of the curve shown in Fig. 1.6 is typical in diode lasers, and this curve is known as light-current, or L-I, curve. I_{th} is measured experimentally as the current where the function that fits the linear part of the L-I curve intercepts the baseline of the output power before lasing (see Fig. 1.6).

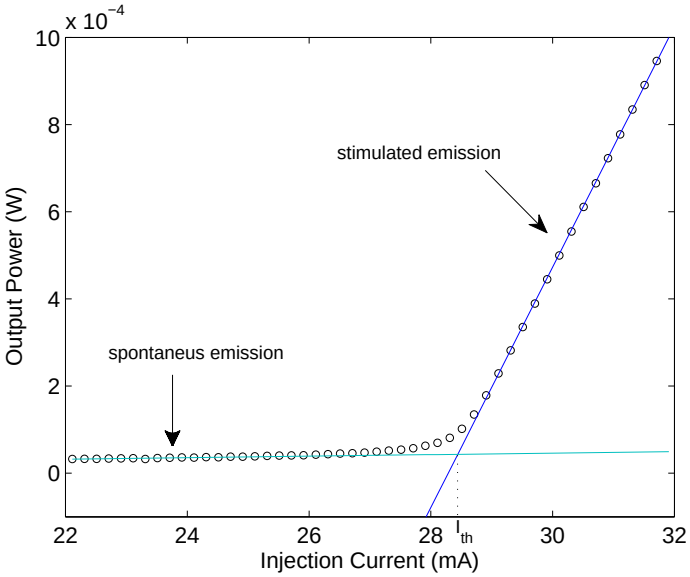

Figure 1.6: Experimental L-I curve for one of the diode lasers used in this thesis (Sony SLD1137VS). Spontaneous emissions dominates the output power before the threshold current (I_{th} = 28.4 mA) is reached, after which the laser starts to lase. Above the threshold the output power increases linearly with the injection current.

Optical Spectrum

FP diode lasers are in general multimode, but depending on cavity design, injection current and temperature of operation, single mode emission can be observed. For lower injection currents the emission is multimode but, as pump current is increased one mode dominates the emission. Figure 1.7 shows the normalized optical spectra for one of the lasers used in this thesis (Mitsubishi ML925B45F) for currents below and well above threshold. Well above threshold (right panel) the emission is almost monomode. Figure 1.8 shows the optical

spectra of another of the lasers used (Hitachi Laser Diode HL6724MG), for three injection currents. We can again see that higher currents favor the dominance of one optical mode.

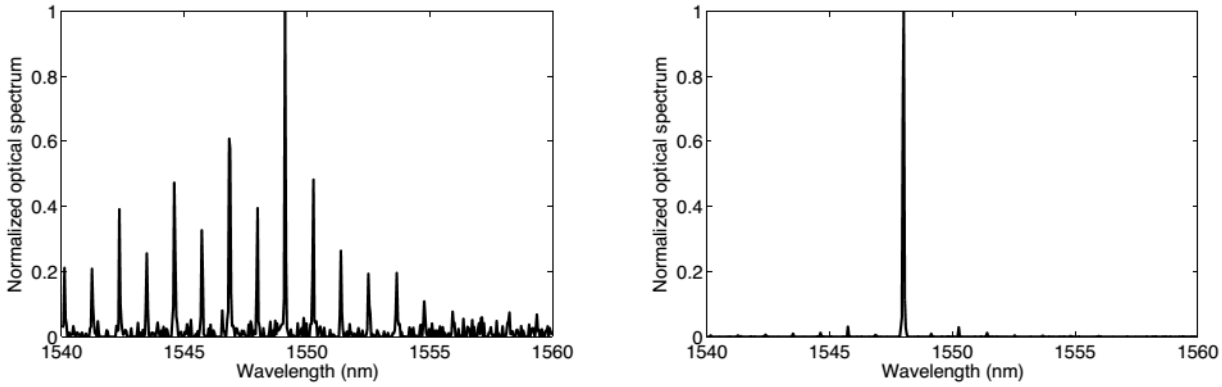

Figure 1.7: Normalized optical spectrum below and well above threshold for one of the FP diode lasers used in this thesis (Mitsubishi ML925B45F). From J. Tiana-Alsina PhD thesis [29].

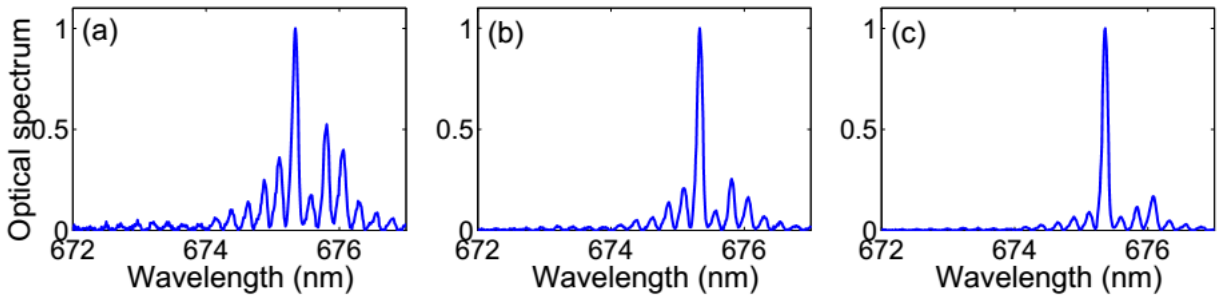

Figure 1.8: Normalized optical spectrum of one of the FP diode lasers used in this thesis (Hitachi Laser Diode HL6724MG) at three pump currents: (a) 29.10 mA, (b) 29.70 mA, and (c) 30.30 mA. Nominal wavelength is 675 nm. From A. Aragoneses PhD thesis [30].

Thermal Effects

Changes in temperature affect substantially the behavior of diode lasers. Increase in temperature leads to higher threshold currents [28]. Also, variations in the temperature cause changes both in the refractive index of the semiconductor material, shifting the cavity modes, and in the band-gap, shifting the maximum gain wavelength. As the shifting in the cavity

modes and the change of the center wavelength of the optical gain are not synchronous, mode-hopping often occur.

Current Modulation, Linewidth Enhancement Factor and Noise

The direct modulation of a diode laser output power through the modulation of its injection current is an important feature that allows a variety of applications. The direct modulation is simple, efficient and fast. It can be achieved by superimposing a signal wave in the injection current.

A small signal modulation can be achieved by superimposing a small sinusoidal current of frequency f_m, to a dc injection current. In this situation the power follows the current modulation up to frequencies near the relaxation oscillation frequency, with a resonant response at f_r [28].

Because the refractive index in the active region depends on the carrier density, the modulation of the carrier density modulates both the power and the refractive index. In consequence current modulation also results in frequency modulation. The ratio of the frequency modulation index to the power modulation index is proportional to the linewidth enhancement factor, α [31]. This quantity is the ratio of the change in the real part of the refractive index n_r with carrier density to the change in the imaginary part of the refractive index n_i with carrier density. It has typical values of 3–5 and is a crucial parameter determining the diode laser dynamics [31]:

$$\alpha \equiv \frac{dn_r/dN}{dn_i/dN}. \tag{1.7}$$

The electric field (and hence the output power) of a semiconductor laser has fluctuations in amplitude and phase which result in power noise and phase/frequency noise. It can be shown that [18] the intensity noise and the frequency noise both broaden as the output power (injection current) increases. The laser linewidth is a Lorentzian with sidebands at the relaxation oscillation frequency. The linewidth is enhanced by a factor $(1+\alpha^2)$ as compared to the classical Schawlow-Townes linewidth [31].

1.2 Semiconductor Lasers with Optical Feedback

The features that distinguish diode lasers from other types of laser (low finesse of the laser cavity, small dimensions, the broad gain curve as a function of the wavelength and the α

factor) conspire to make diode lasers extremely sensitive to the input of external light into the cavity, specially laser light [32]. This light can be fed back to the laser, purposely or not, by an external reflector (optical feedback) or injected from another laser (optical injection).

The effects of optical feedback in diode lasers have attracted attention for more than three decades for being important both for applications and basic research [28, 33]. For applications optical feedback can be either detrimental or beneficial. In optical data recording or optical communications systems the performance of diode lasers is substantially affected by the amount of light fed back from external reflectors such optical disk surfaces and fiber connectors. The sensitivity of diode lasers to optical feedback can also be used to enhance spectral characteristics and to provide tunability for simple, cheap FP diode lasers. External cavities using a frequency selective reflector, usually a diffraction grating, reduce the linewidth, enhance frequency stabilization and permit the continuous tuning of the laser wavelength over many nanometers [34]. Interferometric applications of optical feedback in diode lasers were also developed [35–37], allowing measurements of displacement, distance, vibration and velocity, as well as diode laser diagnostics, through measurements of linewidth [38] and linewidth enhacement factor, α [39].

From a basic research point of view, optical feedback in diode lasers provide an excellent benchmark for optical nonlinear dynamics and chaos studies. Following the dynamical classification of lasers by Arecchi *et al.* [40], diode lasers are class B lasers, and, as we already have seen in section 1.1, the evolution in time of only two variables determine their dynamical behavior. A class B system can oscillate, but it cannot present chaotic dynamics by itself [41]. However, the number of degrees of freedom increase when an external perturbation is applied, such optical feedback, and the system can display chaos. But optical feedback is not only a perturbation. It is a *time-delayed* one, as a consequence of the fact that photons need a finite time to complete a round trip through the external cavity. The re-injection of the 'past state' in the system's present one renders the system infinite dimensional and, thus, opens the door for high-dimensional chaos. The onset of chaos in diode lasers with optical feedback, regarded as fundamental research in the past decades, serve now as basis for many applications (see [42] for a very recent review). Optical feedback is also important for understanding light-matter interactions, testing models and measuring laser parameters [38, 39].

1.2.1 Optical Feedback Regimes and Induced Dynamics

Several parameters determine the type of instability induced by optical feedback.

In 1986 Tkach and Chraplyvy (TC) [43] classified experimentally five regimes of operation, depending on the feedback strength, in terms of both spectral and dynamical properties of the laser emission. Over the years the TC classification became a standard in later research [28,33]. If the feedback strength is very small (feedback fraction of the amplitude less than 0.01%), the linewidth of the laser may become narrow for an adequate relative phase between the emitted and re-injected light, depending also on the feedback fraction [44], this is regime I. Regime II is reached with slightly stronger feedback (< 0.1%): external modes start to play a role and give rise to mode hopping [45]. For an even higher amount of feedback (a narrow region around 0.1%), regime III is reached: mode hopping is suppressed and the laser oscillates with a very narrow linewidth [43]. For regime IV is observed with moderate feedback, (around 1%): the relaxation oscillations become undamped and the linewidth of the laser is highly broadened. Noise level is enhanced largely and coherence collapse (CC) is reached [46]. Regime V occurs for strong feedback (> 10%): external cavity takes over and the laser behaves as if it had a single cavity, resulting in the laser oscillating once more with much narrower linewidth [47,48].

Hirota and Suematsu noted in 1979 that different responses could appear depending on the distance between the laser facet and the external reflector [49]. Regarding the length of the external cavity, two regimes are in general distinguished: the *short cavity* regime, if the feedback delay time is shorter than the relaxation oscillations period (of the order of hundreds of picoseconds) [50,51] and the *long cavity* regime, if the delay time is much longer than the relaxation oscillations period [52].

The operation conditions for all the experiments and simulations presented in this thesis correspond to moderate feedback (regime IV), and *long cavity* regime.

The third parameter that strongly affects the dynamics of diode lasers under optical feedback is the injection current. Besnard *et al.* [53] and Heil *et al.* [54,55] proposed a different classification, depending on the pump current, that distinguishes three main behaviors: stationary regime, low-frequency fluctuation (LFF) regime (see Fig. 1.10) and coherence collapse (CC) regime. The map shown in Fig. 1.9 [54] display the regions where the different

regimes occur, and regions of co-existence, in the parameter space (injection current, feedback strength).

The LFF regime is characterized by sudden power dropouts of the laser intensity. It is a central subject of this thesis and it will be discussed in more in the section 1.3. As the injection current is increased, there is a gradual transition from the LFF regime to the CC regime, the intensity dropouts become more frequent and merge. The CC regime has been identified as a high-dimensional chaotic dynamics and has been studied by using different nonlinear analysis tools such as Poincaré sections, Lyapunov exponents and fractal dimensions [56–58].

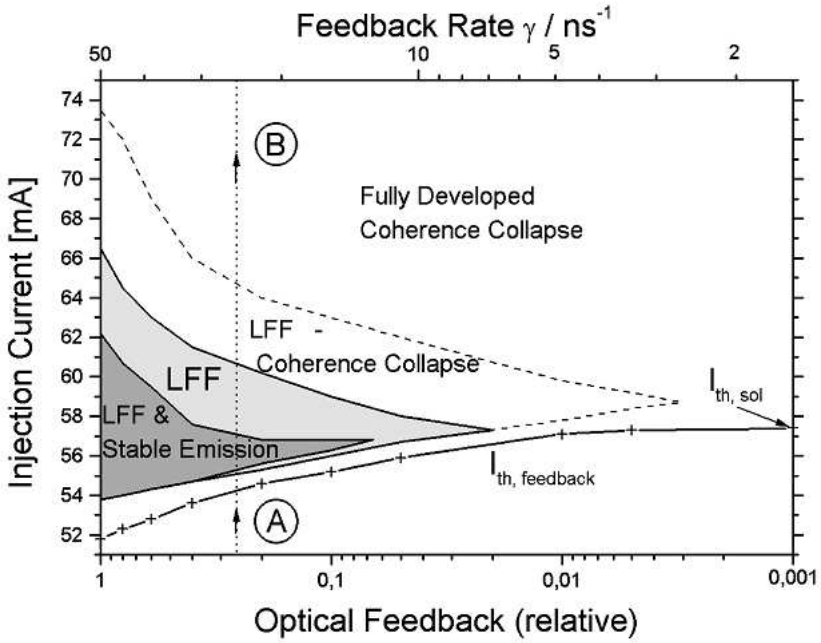

Figure 1.9: Dynamical regimes of a semiconductor laser subject to optical feedback are depicted in the space spanned by feedback strength and injection current. Increasing the injection current along the dotted vertical line from A to B, one can reach every dynamical regime. From Heil *et al.* [54].

1.2.2 The Lang and Kobayashi model

In 1980 a milestone paper was published by Lang and Kobayashi, with a theoretical model to describe the effects of a weak to moderate optical feedback in single-mode diode lasers. The Lang and Kobayashi (LK) model and its generalizations were (and still are) widely used in the

literature. Many predictions of the model were confirmed experimentally and its limitations and properties discussed in numerous works (for example [28,33,59] and references therein).

The LK model represents the light that is fed back to the semiconductor cavity as a time delayed term added to the optical field rate equation. Equation 1.5 for the photon density can be re-written in terms of the complex optical field using $E(t) = \sqrt{S}e^{i\phi(t)}$, where $E(t)$ is the slowly varying field amplitude and $\phi(t)$ is the phase at time t. Adding the delayed term, the field rate equation (in adimensional form) is [60]:

$$\frac{dE}{dt} = \frac{1}{2\tau_p}(1+i\alpha)(G-1)E + \eta E(t-\tau)e^{-i\omega_0\tau} + \sqrt{2\beta_{sp}}\xi, \tag{1.8}$$

where the optical gain is $G = N/(1+\epsilon|E|^2)$. ϵ is a phenomenological saturation coefficient, η is the feedback strength, τ is the feedback delay time and $\omega_0\tau$ is the feedback phase. In the noise term, representing spontaneous emission, β_{sp} is the noise strength and ξ is a complex Gaussian noise with zero mean and unit variance.

The rate equation for the carrier density (in adimensional form) is:

$$\frac{dN}{dt} = \frac{1}{\tau_N}(\mu - N - G|E|^2), \tag{1.9}$$

where μ for the injection current parameter, that is equal to 1 for the threshold of the solitary laser. When we study current modulation, μ is a time-dependent parameter of the carrier density equation, $\mu = \mu_0 + a\sin(2\pi f_{mod}\, t)$, where a is the modulation amplitude, f_{mod} is the modulation frequency and μ_0 is the DC current.

For the simulations presented in this thesis, typical parameters have been used: are always the same. Unless stated, we use: $\epsilon = 0.01$, $\tau_p = 1.67$ ps, $\tau_N = 1$ ns, $\beta_{sp} = 5\times10^{-5}$ ns^{-1}, and $\alpha = 4$. Other parameters have been adjusted to fit the experimental situation (feedback strength, delay time) or have been considered control parameters (μ_0, a, f_{mod}).

In chapters 3 and 4 of this thesis equations 1.8 and 1.9 are numerically integrated to simulate the dynamics of the LFF regime.

1.3 Low-Frequency Fluctuations

Low-frequency fluctuations (LFF) are sudden, apparently random, dropouts of the laser intensity to a very low value. They are observed when the injection current is close to the threshold and the laser is subject to moderate/strong feedback (see Fig. 1.9). The dropout is followed by a slow, step-like recovery of the intensity. As the average frequency of the dropouts (several MHz) is much slower than the characteristic frequencies of the system, the frequency of the relaxation oscillations (a few GHz) or the external cavity frequency (hundreds of MHz), the phenomena are called low-frequency fluctuations. The time duration of the recovery "steps" is the external cavity round trip time [61]. It has been shown that the dropouts are actually the envelope of fast (tens of picoseconds) pulses, observed for the first time with a streak camera by Fischer *et al.* in 1996 [59]. Due to the limited bandwidth of the detection system, these fast pulses, predicted by the LK model [62], have not been observed in the experiments presented in this thesis. Figure 1.10 displays simulated time series showing the fast pulsing dynamics (in black) and the same low-pass filtered data (in red) to simulate the bandwith of the detection system used in the experiments. The results presented in this thesis deal with the slower dynamics of the dropouts, through the analysis of inter-spike intervals (ISIs), the time intervals between consecutive dropouts.

1.3.1 LFF characteristics and origin

The LFF average frequency depends on the injection current, external cavity length and the feedback level. In general, increases linearly with the increase of the injection current. Fig. 1.11 displays, for one of the lasers used in this thesis, time series for three values of the injection current and the average LFF frequency vs. injection current for one of the lasers used in this thesis. The LFF dropouts became more frequent as the injection current increases. If the injection current is further increased the dropouts start to merge as the system approach the fully developed coherence collapse regime. The average frequencies in panel 1.11d were calculated from series with around 100,000 dropouts. The LFF average frequency also decreases linearly with the reflectivity of the external reflector (i.e., with increasing feedback strength) and with the external cavity round trip time (i.e., with increasing feedback delay time) [61, 63]. Also, the magnitude of the dropouts increase with the optical feedback and decrease with the injection current [64].

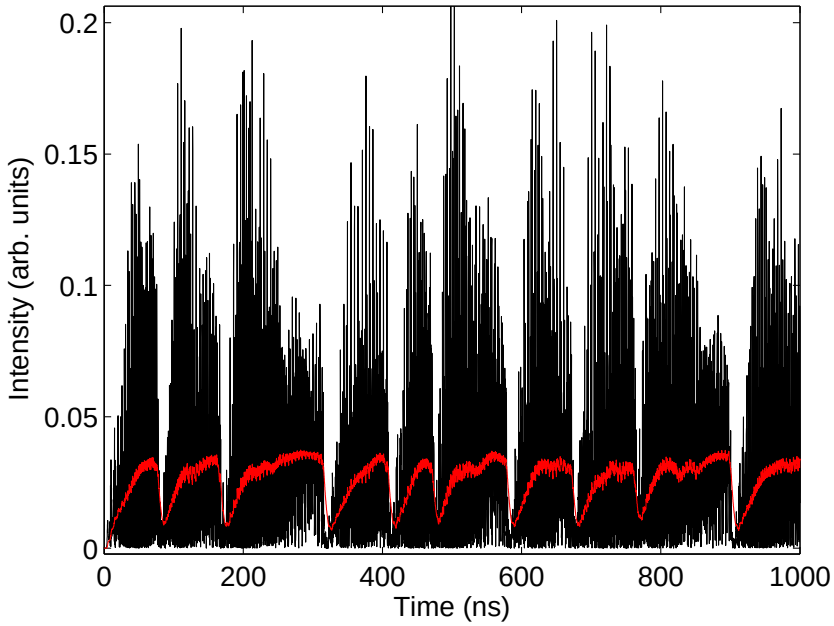

Figure 1.10: Time series simulated numerically with the LK model, equations 1.8 and 1.9. The fast dynamics of the order of picoseconds is shown in black, while the filtered signal, to account for the limited bandwidth of the experimental instruments, is depicted in red. The LFF dropouts can be observed in the filtered trace. Model parameters are: $\mu = 1.005$, $\eta = 10$ ns^{-1}, $\tau = 5$ ns. Other parameters as indicated in subsection 1.2.2.

The LFF regime has been shown to be excitable in certain parameter regions [65–67]. Excitable systems possess a stable stationary state and have a threshold for external perturbations [68, 69]. If the perturbation is smaller than the threshold, the trajectory will return to the stationary state performing a short, linear excursion in its physical variables. If the perturbation is larger than the threshold, the trajectory returns to the stationary state making a large excursion in the phase space manifested by a spike. When the perturbation overcomes the threshold, the amplitude of the spikes becomes independent of the perturbation amplitude. The direct test for excitability consists in verifying the existence of this threshold in the response of the system when a perturbation is applied. An important characteristic of an excitable system is the existence of a refractory time. While the system is performing a spike, it remains insensible to other perturbations.

In the frame of the LK model the LFFs have been explained as the following [70]: in the stable state the most probable external cavity mode for the laser oscillation is the maximum

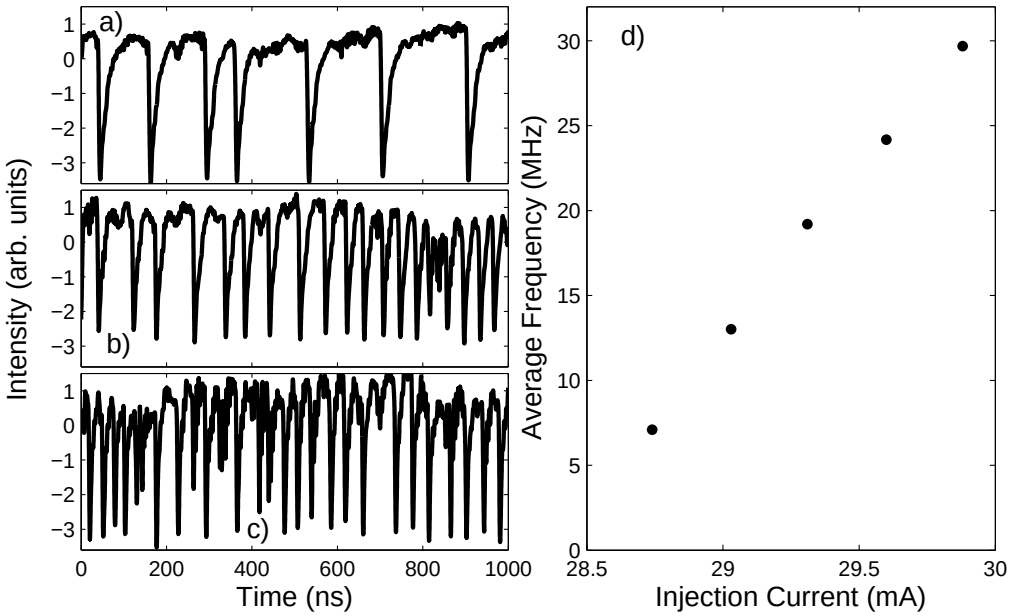

Figure 1.11: As the injection current increases the laser dropouts become more frequent. Panels a) to c) display time series for increasing injection current: a) 28.74 mA, b) 29.31 mA, c) 29.88 mA. d) Average LFF frequency vs. injection current for the Sony SLD1137VS diode laser. In the range of currents used in the experiments with this laser the LFF frequency increases linearly with the injection current. Time delay: 5 ns. Threshold reduction due to feedback: 7.1%. Solitary laser threshold: 28.40 mA.

gain mode (MGM), and at first we suppose that the laser oscillates around the MGM. When the system is close enough to an anti-mode (saddle-point) a collision between the trajectory and the anti-mode can take place. This process corresponds to the power dropout. After that, the laser trajectory begins to recover towards the MGM, being trapped around successive external cavity modes on its way (chaotic itinerancy), until reaching the neighborhood of the MGM. In the vicinity of every cavity mode, the laser make a few cycles, describing chaotic oscillations. Due to noise, the power dropout and the subsequent recovery repeat irregularly in time. As a result, LFFs are observed in the laser output [71, 72]. High resolution measurements of the laser frequency excursion along its mode ellipse (see Fig. 1.12) where reported in [73].

The chaotic itinerancy around the external modes can be visualized in Fig. 1.12 adapted from reference [28].

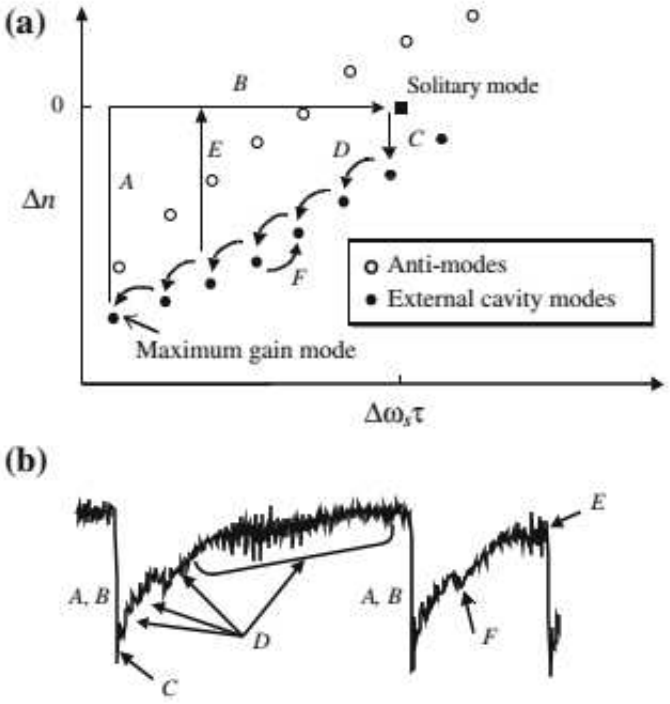

Figure 1.12: a) External- and anti-modes in the phase space of frequency and carrier density. After the collision between the trajectory and an anti-mode, the carrier density increases with constant phase (A), and right after, the phase increases toward the solitary mode (B). A chaotic itinerancy toward the MGM follows (D). b) Corresponding waveform with the steps described in (a). From reference [28].

1.4 Ordinal symbolic analysis

1.4.1 Symbolic Analysis

Symbolic analysis refers to the analysis of series of symbols originated from symbolic transformation of time series. The origin of symbolic analysis goes back to the use of a symbolic description of sequences of geodesic flows on surfaces of negative curvature, by Hadamard, in 1898 [74]. Hadamard discovered a finite set of forbidden patterns (symbol pairs that could not occur) and that the sequences that could exist were the ones that did not contain the forbidden patterns. Morse [75], and after Morse and Hedlund [76], extended this work using a symbolic description to analyze dynamical features such as periodical orbits in classical systems, and referred to the method for the first time as *symbolic dynamics* [77].

Symbolic dynamics, as proposed by Morse and Hedlund [76], is an approach to complex

systems aiming to capture essential aspects of complexity using conceptually simple models [78]. The basic idea is to partition the set of possible states of the system into a finite number of pieces using a symbolic transformation. Each piece is associated with a symbol. If one keeps track of which piece of the state space the system lies in each accessible time interval, the evolution of the system can be described by the sequence of symbols. One have then a "symbolic" dynamical system that reflects and helps to understand the dynamics of the original system citelind:1995.

There are different ways to discretize the available range of original observations and define symbols. It can be based on the Poincaré section [41], that follows a stroboscopic sampling of the multidimensional trajectory of the system in phase-space, giving as result a discrete time mapping, reducing the dimensionality of the problem. The Poincaré section can then be subdivided into cells and assign to all points in each cell the same symbol.

Thresholding criteria can also be used to transform the original data into a sequence of symbols. For example, the original time series can be converted in a series of "ones" and "zeros" depending if the value is higher or lower than a threshold [79,80]. The transformation of the binary sequence into a sequence of more than two symbols, by collecting groups of consecutive symbols, can allow for the inspection of different time scales.

A practical advantage of using symbols is that the efficiency of numerical computations is greatly increased compared with what it would be for the original data. This gain in efficiency can reduce the need for computational resources or enhance understanding. It can also imply speed, which is important for real-time monitoring and control applications. Other advantage is that analysis of symbolic data is often less sensitive to measurement noise. In some cases, experimentalists can accomplish symbolization directly in the instrument by the appropriate design of the sensing elements. Used in combination with appropriate analysis, these "low-resolution" measurements can reduce instrumentation cost and complexity, as pointed out by Daw *et al.* citedaw:2003.

1.4.2 Ordinal analysis

Ordinal analysis [78, 81] is a kind of symbolic analysis in which the symbols are ordinal patterns (OPs), defined through order relations between neighbor values. It was introduced in the context of a new entropy measure, the *permutation entropy*. Roughly speaking, permutation entropy replaces the probabilities of length-D symbol blocks in the definition of the

Shannon entropy [82] by the probabilities of length-D ordinal patterns. The Shannon entropy is defined as the measure of the uncertainty associated to the physical process P, as

$$S[P] = -\sum_{i=1}^{N} p_i \ln(p_i), \tag{1.10}$$

where the probabilities p_i, such that $\sum_{i=1}^{N} p_i = 1$, characterize the process P. For a completely known process, which is predictable with certainty, Shannon entropy is minimum, $S[P] = 0$, while for a uniform distribution, where the knowledge about the system is minimum and all outcomes are equally probable, Shannon entropy is maximum, $S[P] = \ln(N)$, with N being the number of possible outcomes.

Permutation entropy addressed three drawbacks present in Shannon entropy and other classical measures [83]: 1. Shannon and other classical measures do not account for temporal relationships between the values of the time series, so that structure and possible temporal patterns present in the process remains veiled; 2. They often require some previous knowledge about the system; and 3. They are often best designed to deal with linear systems.

As an example of the first drawback, consider a time series with length L. For simplicity consider that the time series contains L different values. For Shannon entropy, equation 1.10, there are $L!$ possible different time series that gives exactly the same value for the measure. Any possible permutation of the elements in the time series yelds the same entropy. The information about the order is completely lost.

In ordinal analysis, the comparison of neighboring values in a time series allows to take into account time causality when constructing the ordinal patterns. The symbolic sequence is determined without any previous knowledge of the system: only, again, by comparing neighbor values. And, finally, the method is useful to describe high-dimensional nonlinear systems [78, 83–85].

Ordinal analysis has been applied in many areas as econophysics, neuroscience, biomedicine and climatology [83, 84, 86].

The first application in the investigation of semiconductor laser dynamics is from 2010. J. Tiana-Alsina *et al.* [87] used ordinal analysis to characterize the LFF dynamics. They computed the entropy and the statistical complexity measure previously introduced by Martin

et al. [88] via ordinal patterns. They found a trasition in the dynamics, as the pump current is increased, characterized by a reduction of the permutation entropy accompanied by an increase of the statistical complexity, which is robust to the size of the data sets and the dimension of the ordinal patterns. Rubido *et al.* [89] applied ordinal analysis to characterize the dynamics of the LFF regime for a wide range of pump current values. They found that for low pump currents the dropouts have no correlations, as all the words were equally probable; but for higher pump currents, correlations between consecutive dropouts appear. They also compared predictions of the LK model with the phenomenological model introduced by Eguia *et al.* [90], and found that the LK model reproduces better the temporal correlations present in the system.

Soriano *et al.* [91] and Zunino *et al.* [92] also estimated the permutation entropy, together with the permutation statistical complexity, of a semiconductor laser with feedback in the chaotic regime. By analyzing these quantifiers as a function of the embedding dimension, they identified the relaxation oscillation period and the feedback time delay. Xiang *et al.* [93] used the permutation entropy to study the unpredictability of the chaotic dynamics of a laser diode with polarization-preserved and polarization-rotated feedback. Toomey and Kane [94] estimated the permutation entropy of a laser diode with optical feedback for different feedback strengths and pump currents, showing the different degrees of complexity in a two-dimensional parameter space (optical feedback and pump current). They showed that the degree of complexity is sensitive to the delay used to compute the ordinal patterns. Toomey *et al.* [95] have shown that permutation entropy and a variation of it called weighted permutation entropy (WPE), that also incorporates amplitude information [96], can be used to identify pulsed dynamics in different laser systems and serve as relative measures of noise in pulses amplitude and period.

In this thesis we analyze statistics of OPs in ISI time series of lasers with optical feedback in the LFF regime. In the following we present how the ordinal patterns are constructed.

Ordinal Patterns

In chapters 2–4 we will analyze experimental and simulated ISI sequences employing ordinal analysis. By analyzing the statistics of the different ordinal patterns, it can capture subtle variations in temporally correlated data [87].

Each ISI sequence, $\{\Delta T_i\}$, is transformed into a sequence of ordinal patterns (OPs), which are defined by considering the relative length of D consecutive ISIs and assigning them a symbol that indicates their relative length, in the same order as they appear in the sequence, as shown in figure 1.13. The shortest interval is assigned 0 and the longest interval is assigned $D-1$. For $D=2$ the only two possibilities are: $\Delta T_i > \Delta T_{i+1}$ that gives the '10' OP, and $\Delta T_i < \Delta T_{i+1}$ that gives the '01' OP. For $D=3$ there are six possibilities: $\Delta T_i < \Delta T_{i+1} < \Delta T_{i+2}$ gives '012', $\Delta T_{i+1} < \Delta T_i < \Delta T_{i+2}$ gives '102', and so on. The OP probabilities are then calculated by counting their frequency of occurrence in the sequence.

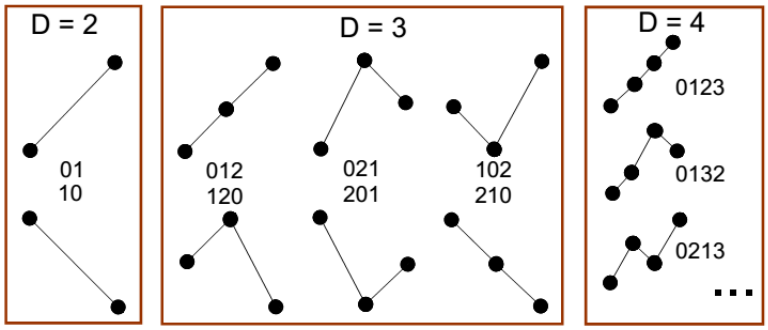

Figure 1.13: Schematic representations of the ordinal patterns (OPs) of dimension $D=2$, $D=3$, and three examples of OPs of dimension $D=4$. This figure is a courtesy of A. Aragoneses.

We also compute the transition probabilities (TPs) from an OP to another OP [97]. The TPs are normalized such that all possible transitions from one OP sum one. To fix the ideas, for $D=2$ OPs, $\mathrm{TP}_{01\to01}+\mathrm{TP}_{01\to10}=1$ and $\mathrm{TP}_{10\to01}+\mathrm{TP}_{10\to10}=1$.

The symbolic transformation employed here disregards the information about the precise duration of the ISIs, what renders the method very robust against noise, but it keeps the information about temporal correlations among them, i.e., about correlations in the timing of the optical spikes. Specifically, in the next chapters we will analyze correlations among 3 spikes (by using $D=2$ OPs), 4 spikes (by using $D=3$ OPs) and 5 spikes (by using $D=2$ TPs or $D=4$ OPs). As the number of possible OPs increases as $D!$, the TP method has the advantage of allowing to infer the presence of correlations among 5 consecutive spikes by computing only 2 TPs ($\mathrm{TP}_{01\to01}$ and $\mathrm{TP}_{10\to10}$) instead of computing the probabilities of $4!=24$ OPs.

Chapter

2

Ordinal Analysis of the Dynamics of Semiconductor Lasers in the LFF Regime

In this chapter we analyze the dynamics of semiconductor lasers when they operate in the LFF regime induced by optical feedback. By using symbolic analysis we unveil a nontrivial organization of ordinal patterns, revealing serial spike correlations. The probabilities of the patterns display a well-defined, hierarchical and clustered structure. We also consider the influence of direct current modulation and identify clear changes in the dynamics as the modulation amplitude increases. To confirm the robustness of the observations the experiments were performed using different lasers under different feedback conditions. Simulations of the Lang and Kobayashi (LK) model, including spontaneous emission noise, are found to be in good agreement with the observations, providing an interpretation of the correlations present in the dropout sequence as due to the interplay of the underlying attractor topology, the periodic modulation, and the noise that sustains the dropout events.

The results presented in this chapter were published in references [97, 98]. The experiments were performed in collaboration with Andrés Aragoneses, a former PhD student in the DONLL group. The simulations of the LK model (not shown here) were performed by Sandro Perrone, another former PhD student in the DONLL group.

2.1 Experimental Setup

2.1.1 No Modulation

The experimental setup used in the experiments without modulation is presented in Fig. 2.1. The experiments were performed with a 675 nm Al-GaInP semiconductor laser (AlGaInP Sanyo DL-2038-023) with optical feedback from a diffraction grating. The external cavity length was 70 cm, giving a feedback delay time of 4.7 ns. A beam-splitter sends 50% of the light to a 1 GHz oscilloscope (Agilent Infiniium 9000). The laser temperature and pump current were controlled to an accuracy of 0.01 C and 0.01 mA respectively with a ITC502 Thorlabs laser diode combinator controller. The operating temperature was 18 C and the laser pump current was varied in steps of 0.1 mA, from 26.3 mA to 27.3 mA. At 18 C the threshold current of the solitary laser is $I_{th} = 27.8$ mA, and the feedback-induced threshold reduction is 6.5%. Time series of 32 ms were recorded (3.2×10^7 data points), containing 70,000–300,000 spike events, for low and high pump current respectively.

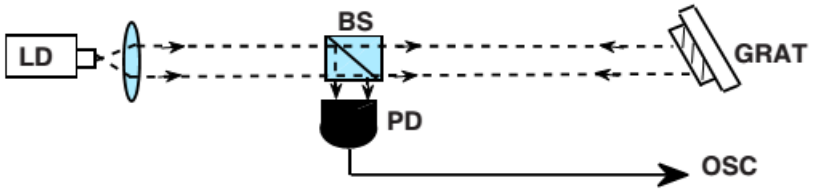

Figure 2.1: Experimental setup, where LD stands for laser diode, BS for beamsplitter, PD for photodetector, OSC for oscilloscope and GRAT for grating.

2.1.2 With Modulation

Two setups with very different time delays were employed. One propagating in air, emitting at 650 nm, optical storage (DVD) wavelength; another propagating through fiber, emitting at 1550 nm, telecom wavelength. The experimental setups are schematically shown in Fig. 2.2.

For the 650 nm laser, the external cavity is 70 cm (giving a feedback time delay of 4.7 ns) and the feedback threshold reduction is 8%. A 50/50 beam-splitter sends light to a photodetector (Thorlabs DET210) connected with a 1 GHz oscilloscope (Agilent DSO 6104A). The solitary threshold is $I_{th} = 38$ mA and the current and temperature (17 C) are stabilized with an accuracy of 0.01 mA and 0.01 C, respectively, using a controller (Thorlabs ITC501). Through

a bias-tee in the laser head, a sinusoidal RF component from a leveled waveform generator (HP Agilent 3325A) is combined with a constant DC current of 39 mA. The modulation frequency is f_{mod} = 17 MHz and the modulation amplitude varies from 0 mV to 78 mV in steps of 7.8 mV (from 0% to 4% of the dc current in steps of 0.4%). For each modulation amplitude, five measurements of 3.2 ms were recorded. The time series contains between 74,000 and 207,000 dropouts, at low and high modulation amplitude, respectively.

For the 1550 nm laser, the time delay is 25 ns and feedback threshold reduction is 10.7%. The solitary threshold is 11.20 mA, the dc value of the pump current is 12.50 mA, the modulation frequency is fmod = 2 MHz and the modulation amplitude varies from 0 mV to 150 mV in steps of 10 mV (from 0% to 24% of the DC current in steps of 1.6%). The time series contain between 8,000 and 19,000 dropouts, at low and high modulation amplitude, respectively. While, for the 1550 nm laser, the modulation frequency is about one order of magnitude smaller than for the 650 nm laser, the relation with the characteristic time-scale of the LFF dynamics, given by the average inter-spike interval $\langle \Delta T \rangle$ is about the same: for the 650 nm laser, $\langle \Delta T \rangle$ = 365 ns and thus $\langle \Delta T \rangle \times f_{mod}$ = 6.2. For the 1550 nm laser, $\langle \Delta T \rangle$ = 2.55 μs and $\langle \Delta T \rangle \times f_{mod}$ = 5.1.

2.2 LFF Symbolic Dynamics without Current Modulation

Figure 2.3 displays the probabilities of the six possible words for D = 3 (indicated in the panel in the right of the figure), computed from time-series recorded within a wide range of pump currents. The symbolic analysis reveals that serial correlations among four consecutive spikes are present in the spike sequence: if there are no correlations (null hypothesis, represented as gray region in Fig. 2.3), the six words are equally probable; however, in Fig. 2.3 one can observe that the probabilities are clearly not consistent with the null hypothesis.

We can also observe a hierarchy in the probability values, which presents a crossover at about 26.6 mA: for higher pump currents the most probable word is '210' corresponding to three consecutively decreasing inter-spike intervals), while for lower pump currents, the most probable word is '012' (corresponding to three consecutively increasing intervals).

Figure 2.3 also reveals a clustered organization of the probabilities: words '021' and '102', on the one hand, and words '120' and '201', on the other hand, occur with similar probability. The probabilities of these two pairs of words present the same evolution when the pump

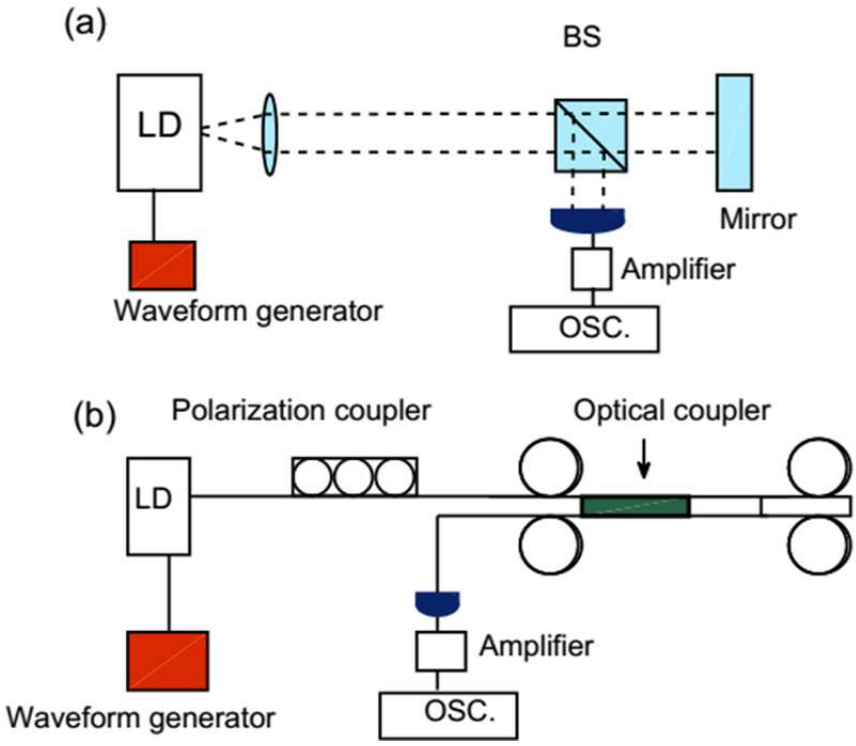

Figure 2.2: Experimental setup for (a) 650 nm laser (Hitachi HL6714G) and (b) 1550 nm laser (Mitsubishi ML925B45F). LD stands for laser diode, BS for beam-splitter and OSC for oscilloscope.

current is varied. The robustness of these findings was confirmed by using different lasers and feedback conditions, where the same clustered hierarchical structure was found.

2.3 LFF Dynamics with Current Modulation

2.3.1 ISI Distributions and Return Maps

Figure 2.4 displays the intensity time series, the probability distribution functions (PDFs) of inter-spike intervals, ΔT (ISIs), and the return maps, ΔT_i vs ΔT_{i+1}, for four modulation amplitudes for the 650 nm laser. As it has been reported in the literature the dropouts tend to occur at the same phase in the drive cycle with current modulation, and the ISIs are multiples of the modulation period [65, 99, 100]. For increasing modulation amplitude, the ISIs become progressively smaller multiples of the modulation period and, for high enough modulation amplitude, the power dropouts occur every modulation cycle [99]. Here, for the highest modulation amplitude, the PDF presents a strong peak at two times the modulation pe-

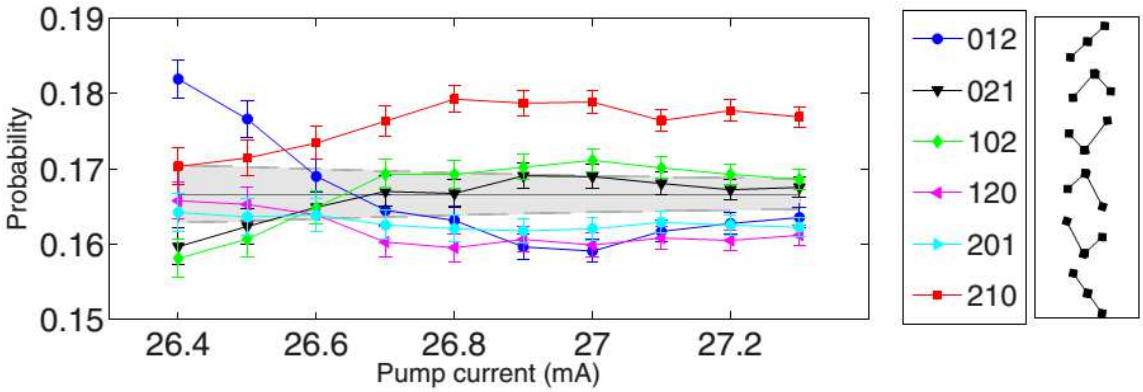

Figure 2.3: Probabilities of the six words (schematically indicated in the right panel) vs the laser pump current. Two clusters of words can be observed, with similar probabilities: '021'-'102' (black-green) and '120'-'201' (magenta-cyan). A crossover in the hierarchical organization of the words occurs at about 26.6 mA: at lower current values the word '012' (blue) is the most probable one, while at higher currents values, the word '210' (red) is the most probable one. The error bars are estimated with a binomial test and the gray region indicates probability values consistent with the null hypothesis that there are no correlations in the spike sequence, and therefore, the six words are equally probable.

riod [see Fig. 2.4(k)]. The return maps (third column of Fig. 2.4) display a clustered structure, with "islands" that correspond to the well-defined peaks observed in the PDFs, also in good agreement with previous reports [65, 99]. A similar behavior is observed with the 1550 nm laser (Fig. 2.5). The plots of ΔT_i vs ΔT_{i+1} are almost symmetric, suggesting that $\Delta T_i > \Delta T_{i+1}$ and $\Delta T_i < \Delta T_{i+1}$ are equally probable; however, in the next section we will demonstrate that the modulation induces correlations in the ΔT sequence, induced by the modulation, which can not be inferred from these plots.

2.3.2 Symbolic Dynamics

Figure 2.6 shows the probabilities of words of $D = 2$ (a, b) and $D = 3$ (c, d), vs. the modulation amplitude, for the 650 nm laser (a, c), for the 1550 nm laser (b, d). The gray region indicates probability values consistent with the null hypothesis (NH) that the words are equally probable, and thus, that there are no correlations among the dropouts. In other words, probability values outside the gray regions are not consistent with a uniform distribution of word probabilities and reveal serial correlations in the ISI sequence. It can be noticed that the gray

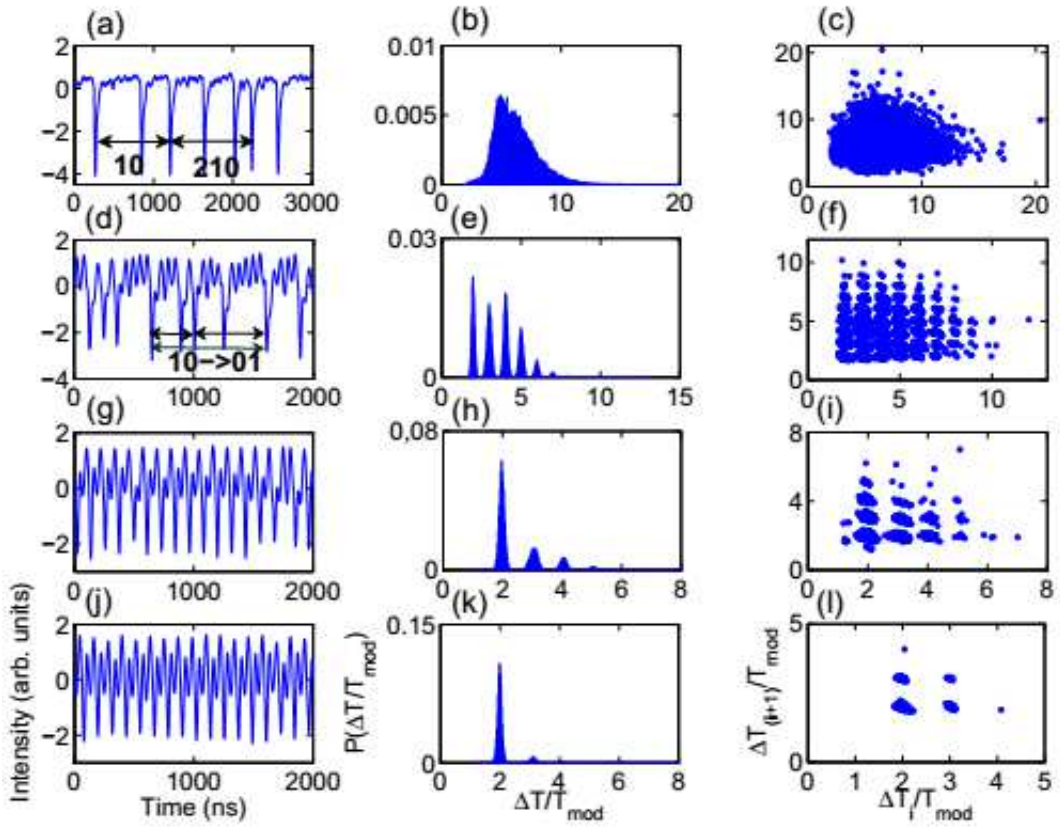

Figure 2.4: Time traces of the laser intensity (650 nm laser), probability distribution functions (PDFs) of the inter-spike intervals, ΔT_i (ISIs), and return maps ΔT_i vs ΔT_{i+1} in units of the modulation period (T_{mod}) for increasing modulation amplitude, from top to bottom: no modulation, 23.4 mV (1.2%), 31.2 mV (1.6%), and 39.0 mV (2%). In panel (a) the words '10' (D = 2) and '210' (D = 3) are depicted as examples; in panel (c) the transition '10' → '01' is depicted as example.

region is narrower in (a, c) than in (b, d). This is due to the fact that the number of dropouts recorded for the 650 nm laser is much larger than for the 1550 nm laser (the corresponding delay times being 4.7 ns and 25 ns respectively).

It is observed that the dynamics is consistent with the NH, in the case of $D = 2$, for small and for high modulation amplitude. However, the analysis with $D = 3$, reveals that, for high modulation, the probabilities are outside the gray region, revealing correlations among four consecutive ISIs. We note that there are two groups of words, one less probable ('012', '210') and one more probable ('021','102', '120', '201'), resulting, for $D = 2$, in the same probabilities

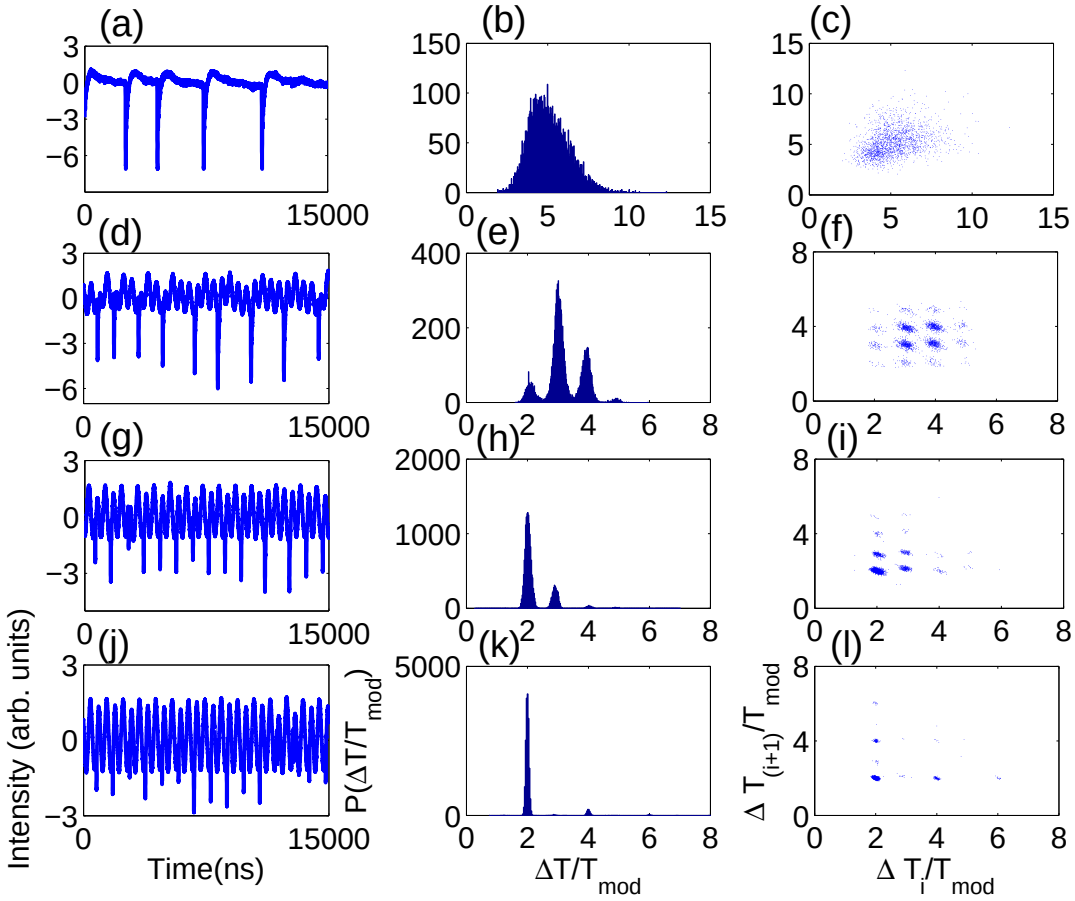

Figure 2.5: As Fig. 2.4 but for the data recorded from the 1550 nm wavelength laser. Left column: time traces of the laser intensity; middle column: PDFs of the inter-spike intervals, ΔT_i; right column: return maps ΔT_i vs ΔT_{i+1} in units of the modulation period (T_{mod}). First row: no modulation; second row: modulation amplitude of 40 mV (6.4% of the DC current); third row: 80 mV (12.8%); forth row: 120 mV (19.2%). From A. Aragoneses PhD thesis [30].

for '01' as for '10'. With $D = 3$, the less probable words are those which imply three consecutively increasing or decreasing IDIs and this can be understood in the following terms: strong enough modulation forces a rhythm in the LFF dynamics, and three consecutively increasing or decreasing intervals imply a loss of synchrony with the external rhythm, and thus, are less likely to occur.

By computing the four transition probabilities of $D = 2$ words, depicted in Fig. 2.7, we obtain information about correlations among five consecutive dropouts. This analysis is statistically more robust than computing the probabilities of the 24 words of length $D = 4$.

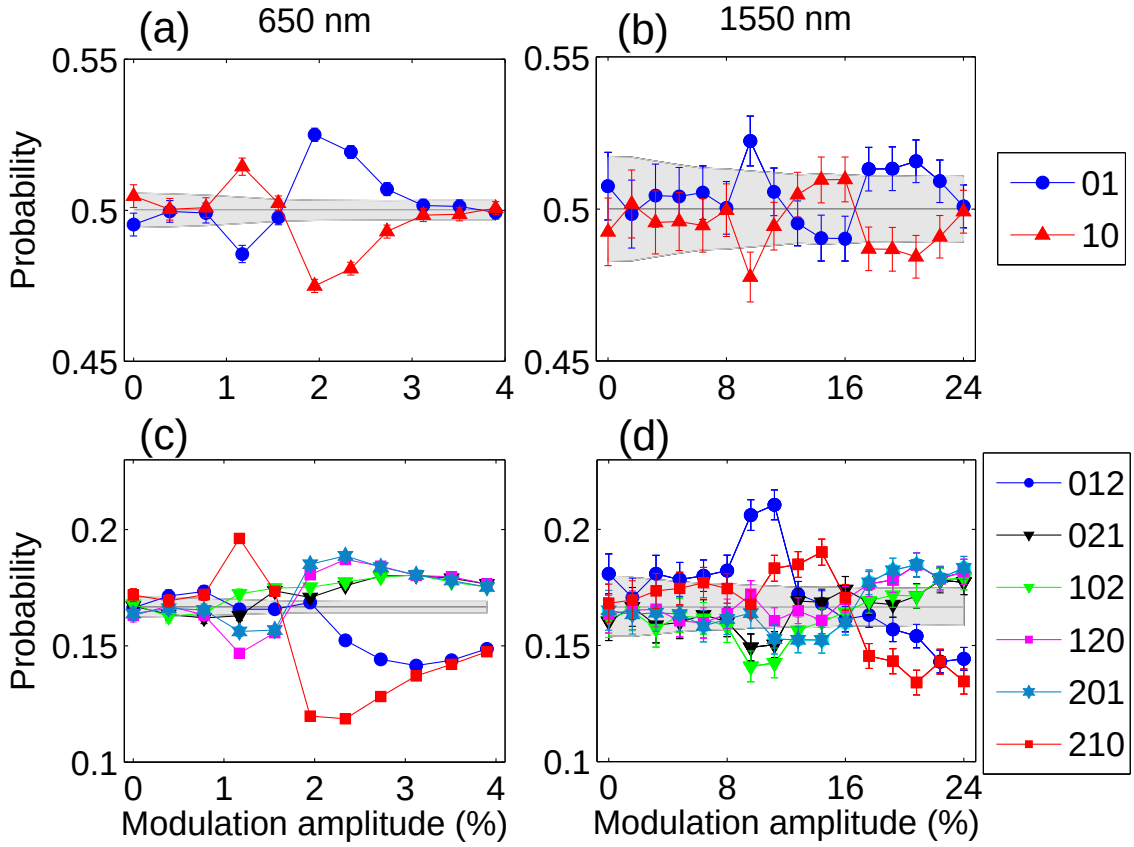

Figure 2.6: Probabilities of the words of D = 2 (a, b) and D = 3 (c, d) versus the modulation amplitude for the experiment with the 650 nm laser (a, c), the experiment with the 1550 nm laser (b, d). The gray region ($p \pm 3\sigma$, where $p = 1/D!$, $\sigma = \sqrt{p(1-p)/N}$, and N is the number of words in the symbolic sequence) indicates probability values consistent with 95% confidence level with the null hypothesis that all the words are equally probable (i.e., that there are no correlations present in the sequence of dropouts).

The results in Fig. 2.7 confirm that, at this time scale, the dynamics is still consistent with the NH for low modulation amplitudes but, as the modulation increases, a transition takes places and the transition probabilities (TPs) display a deterministic-like behavior. This transitions occur at the same values as in Fig. 2.6 (at about 1.8% modulation amplitude for the 650 nm case, 16% for the 1550nm). Figure 2.7 shows that, for high modulation amplitude, the most probable transitions are those which go from one word to the same word ('01' → '01' and '10' → '10'), because the external forcing imposes a periodicity in the LFF dynamics. The transition in the dynamics, and the qualitative agreement between the two lasers, are

independent of the type of normalization used to compute the TPs.

Within the framework of the LK model, the LFF dynamics is sustained by spontaneous emission noise, and thus, one could expect weak correlations in the sequence of dropouts. While this is indeed the case for no modulation or very weak modulation amplitude, larger modulation induces precise correlations, which are adequately reproduced by the LK model. For strong modulation the reason why some words and transitions are more probable than the others is well understood (as due to the external rhythm imposed by the modulation), but for no modulation and also for moderate modulation amplitude, further investigations are needed in order to understand the symbolic behavior.

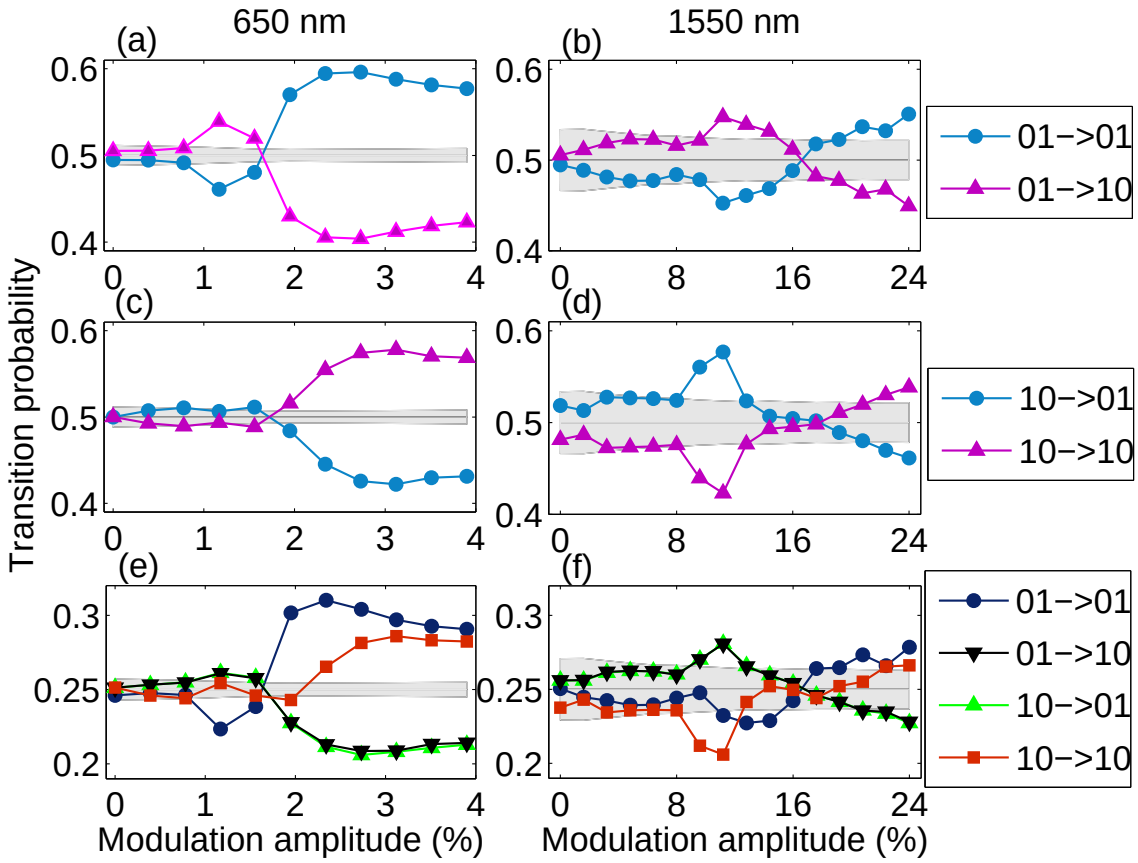

Figure 2.7: Transition probabilities for the 650 nm laser (a, c,e), and the 1550 nm laser (b,d,f). In the first two rows the panels display probalities from one word to the same or to the other, and these two probabilities sum one, as explained in section 1.4. The normalization used in the third row consideres all four transitions such that $TP_{(01\to01)} + TP_{(01\to10)} + TP_{(10\to01)} + TP_{(10\to10)} = 1$.

2.4 Conclusions

We have studied experimentally the symbolic dynamics of a semiconductor laser with optical feedback and current modulation in the LFF regime. We have analyzed time series of inter-spike intervals employing a symbolic transformation that allows us to identify clear changes in the dynamics induced by the modulation. For weak modulation the sequence of dropouts is found to be mainly stochastic, while for increasing modulation it becomes more deterministic, with correlations among several consecutive dropouts. We have identify clear changes in the probabilities of the symbolic words and transitions with increasing modulation amplitude. We speculate that the symbolic behavior uncovered here is a fingerprint of the underlying topology of the phase space, and is due to the interplay of noise-induced escapes from an stable external cavity mode, and the dynamics in the coexisting attractor. In the next chapters we will analyze the influence of varying the modulation frequency and the natural (without modulation) spike rate.

The methodology proposed here can be a useful tool for identifying signatures of determinism in high-dimensional and stochastic complex systems. It provides a computationally efficient way to unveiling structures and transitions hidden in the time series. As the laser in the LFF regime is an excitable system, our results could be relevant for understanding serial correlations in the spike sequences of other forced excitable systems.

Chapter

3

Influence of the Modulation Frequency on the Symbolic Dynamics of the Laser

In this chapter we investigate how the spiking laser output represents a weak periodic input that is implemented via direct modulation of the laser pump current. We focus on understanding the influence of the modulation frequency. Experimental sequences of inter-spike-intervals (ISIs) are recorded and analyzed by using the ordinal symbolic methodology that identifies and characterizes serial correlations in datasets. The change in the statistics of the various symbols with the modulation frequency is empirically shown to be related to specific changes in the ISI distribution, which arise due to different phase-locking regimes. A good qualitative agreement is also found between simulations of the Lang and Kobayashi model and experimental observations. This methodology is an efficient way to detect subtle changes in noisy correlated ISI sequences and may be applied to investigate other optical excitable devices. The results presented in this chapter have been published in reference [101]. The experiment described here was performed in collaboration with Carlos Quintero-Quiroz.

3.1 Experimental Setup

The experimental setup used here is similar to that shown in Fig. 2.2a. A semiconductor laser (Sony SLD1137VS), with a solitary threshold current I_{th} =28.4 mA, temperature- and

current-stabilized with an accuracy of 0.01 C and 0.01 mA, respectively, using a combi controller (Thorlabs ITC501), emitting at 650 nm, has part of its output power fed back to the laser cavity by a mirror 70 cm apart (the external cavity round-trip time is 4.7 ns). A 50/50 beamsplitter in the external cavity sends light to the detection branch consisting of a photodetector (Thorlabs DET210) connected to an amplifier (FEMTO HSA-Y-2-40) and a 1 GHz digital storage oscilloscope (Agilent Technologies Infiniium DSO9104A). A neutral density filter in the external cavity allows to control the feedback power. The DC pump current is I_{DC} =29.10 mA, the laser is operated at 19.00 C and a threshold reduction due to feedback of 7% is observed.

Through a bias-tee in the laser mount, the pump current is modulated with a sinusoidal signal provided by a waveform generator (Agilent 33250A), with frequency varying from 1 to 50 MHz in steps of 1 MHz, and a peak-to-peak amplitude varying from 0.8% to 2% of I_{DC}, in steps of 0.4%. For these modulation amplitudes the laser current is always above the solitary threshold. The experiment is controlled by a LabVIEW program that acquires the time series, detects the spikes, and calculates the inter-spike-intervals (ISIs) until 40,000 ISIs are recorded. Then, the program changes the modulation frequency and/or amplitude, waits a few seconds to let transients die away, and the process is repeated.

3.2 Experimental Results

Figure 3.1 displays the measured intensity time series and the ISIs distribution for six values of the modulation frequency, f_{mod}, when the modulation amplitude is 1.2% of I_{DC}. For each frequency 30 modulation cycles are shown. The ISI distribution is computed with bins centered at integer multiples of T_{mod} (with the exception of the first bin, centered in 0). The modulation frequencies displayed are chosen to highlight different behaviors: either $n:1$ locking predominates (revealed by a high peak in the ISI distribution at nT_{mod}), or there is a transition from $n:1$ to $n+1:1$ locking, revealed by the peaks at nT_{mod} and $(n+1)T_{mod}$ having nearly the same heights.

For f_{mod} = 7 MHz (first row) the ISI distribution peaks at T_{mod}. The time series reveals that the ISIs are in fact heterogeneous, as in this case the bin centered in T_{mod} is about 143 ns wide. As the modulation frequency increases, the peak in the ISI distribution shifts to higher multiples of T_{mod} and the ISIs become more homogeneous. At 26 MHz (third row)

phase locking 2:1 occurs with 3:1 intermittency. In the time series one can notice that, after a dropout occurs in a modulation cycle, the next cycle takes place during the intensity recovery time, and the consecutive spike is separated in time by $2T_{mod}$. Similar observation holds for higher frequencies, now other modulation cycles being clearly visible in the intensity oscillations between consecutive spikes. For 39 MHz (fifth row) the 3:1 pattern is dominant and for 49 MHz (sixth row) we can see intermittent switching between 3:1 and 4:1. As the frequency increases and the modulation becomes faster, the ISIs become larger multiples of T_{mod} as the dropouts are spaced by an increasing number of cycles.

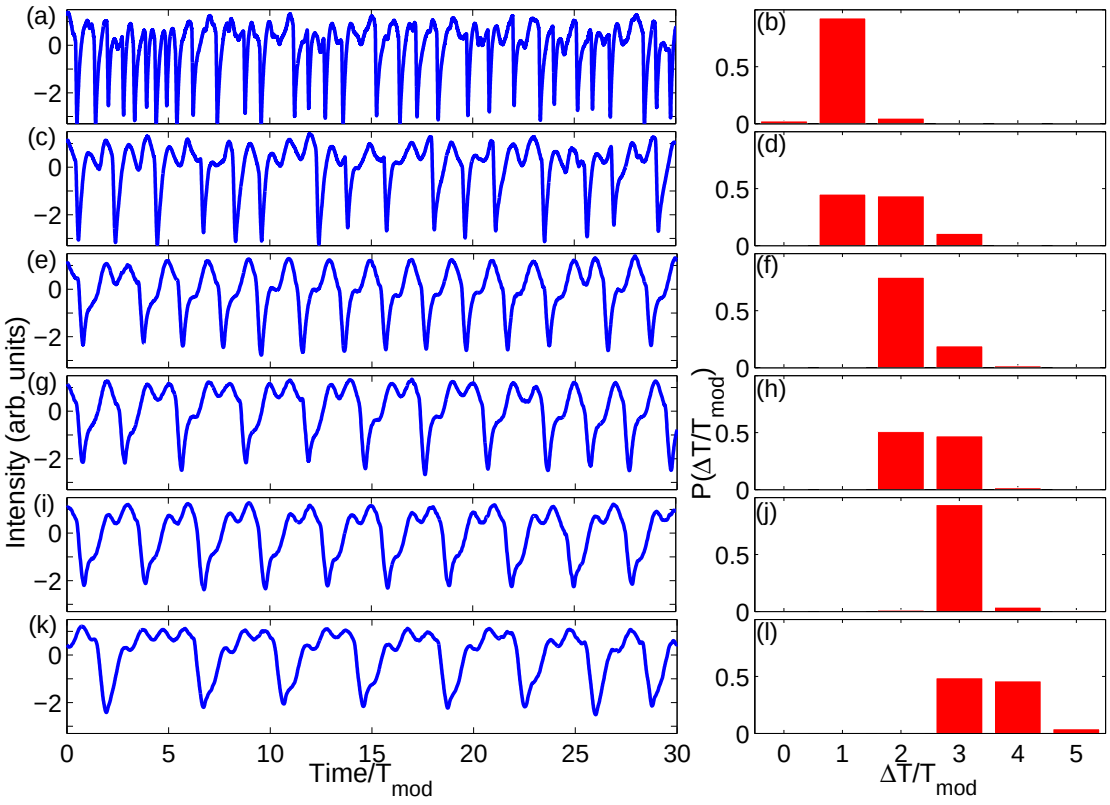

Figure 3.1: Experimental time series of LFF intensity spikes (left column) and the corresponding inter-spike-interval (ISI) distribution (right column). The modulation amplitude is 1.2% of I_{DC} and the modulation frequency is 7 MHz (a-b); 14 MHz (c-d); 26 MHz (e-f); 31 MHz (g-h); 39 MHz (i-j); 49 MHz (k-l). In the left panels only 30 modulation cycles are shown, but the ISI distributions in the right panels are computed from 40000 ISIs.

Figure 3.2 displays the variation of the mean ISI, $< \Delta T >$, with the forcing frequency. In panel 3.2a we plot $< \Delta T >$ as a function of f_{mod} for four modulation amplitudes (indicated as percentages of I_{DC}). A decreasing trend can be observed, interrupted by "plateaus" where

$< \Delta T >$ oscillates (at about 30 MHz) and remains nearly constant (at about 45 MHz) for the two lower amplitudes, or continues to decrease for the higher amplitudes.

The origin of this behavior can be identified in Fig. 3.2(b), where the ratio $< \Delta T > / T_{mod}$ is plotted vs. the modulation frequency. After an almost linear increase for low modulation frequencies (where $< \Delta T >$ varies very little compared to T_{mod}), two plateaus occur at $< \Delta T > / T_{mod} \sim 2$ and $< \Delta T > / T_{mod} \sim 3$. For strong modulation amplitude the shape of the plateaus become more clear, while for weak modulation, only signatures of the plateaus are evident.

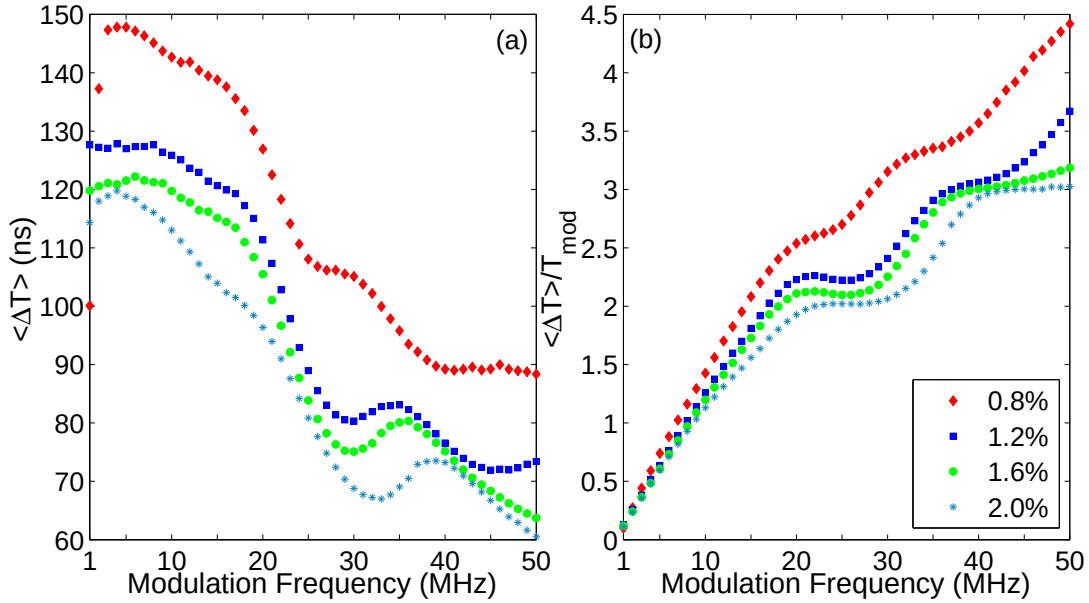

Figure 3.2: (a) Mean ISI as a function of the modulation frequency when the modulation amplitude is 1.2% of I_{DC}. (b) Ratio between the mean ISI and the modulation period, $< \Delta T > / T_{mod}$, versus modulation frequency for several modulation amplitudes.

To investigate if the changes in the ISI distribution induced by the variation of the modulation frequency occur smoothly or rather abruptly, the probabilities of the first 5 bins [i.e., p_n with $n = 0 \ldots 4$, p_n being the probability of an ISI interval being in the bin $(nT_{mod} - T_{mod}/2, nT_{mod} + T_{mod}/2)$] are plotted vs. f_{mod}. Figure 3.3 displays the results for the same modulation amplitude as in Fig. 3.1 (1.2%). A smooth variation of the probabilities is observed over the entire frequency range. For clarity we indicate with vertical arrows the six frequencies corresponding to the panels in Fig. 3.1. It can be observed that p_1 displays a maximum (close to 1) at 7 MHz, p_2, at 26 MHz and p_3, at 39 MHz, while $p_1 \sim p_2$ at 14 MHz, $p_2 \sim p_3$ at 31 MHz and $p_3 \sim p_4$ at 49 MHz.

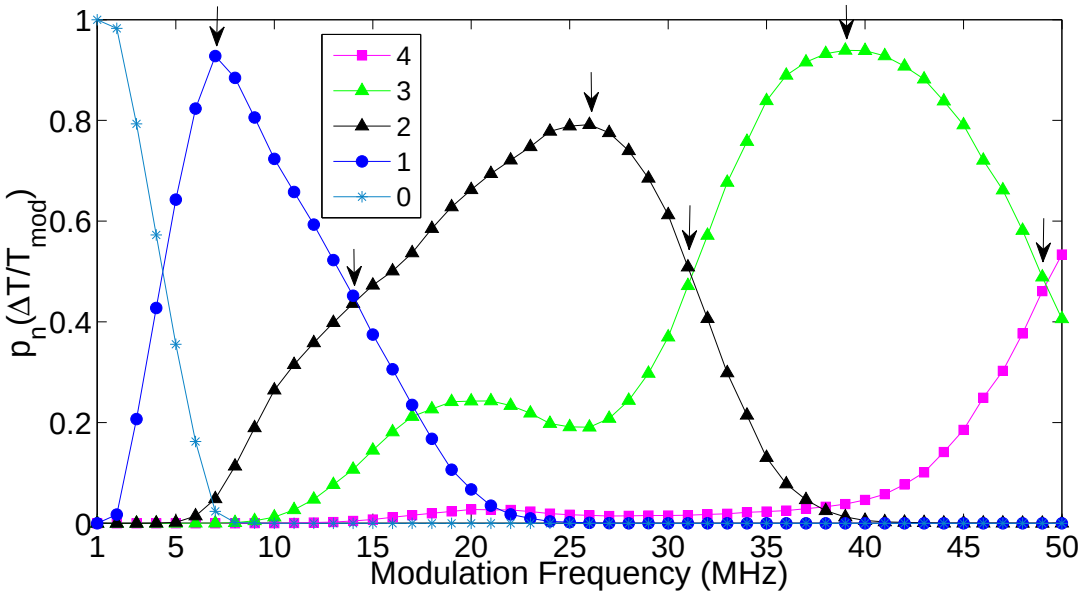

Figure 3.3: Probability, p_n, that an ISI value is within the interval $nT_{mod} - T_{mod}/2, nT_{mod} + T_{mod}/2$. n values in the legend. The first five probabilities are shown, for the same modulation amplitude as Fig. 1 (1.2%).

Figure 3.4 displays the results of ordinal analysis applied to the ISI sequences, for the same modulation amplitude. We present results for $D = 2$ and $D = 3$. For $D = 2$ [Fig. 3.4(a)] we plot simultaneously three probabilities: the probability of one OP ['01', as the probability of '10' is 1-P('01')] and the probabilities of two transitions (from one OP to the same OP, as the other two TPs can also be readily calculated from the normalization conditions: $TP_{01\rightarrow01}+TP_{01\rightarrow10} = 1$ and $TP_{10\rightarrow01}+TP_{10\rightarrow10} = 1$). For $D = 3$ [Fig. 3.4(b)] we plot simultaneously the probabilities of the 6 OPs.

We can see smooth changes in these probabilities as the modulation frequency varies. The same type of smooth variation that was observed in the p_n probabilities (Fig. 3.3), is seen here, more clear in the $TP_{01\rightarrow01}$ and in the OP '210' probability (red curves). These probabilities are the ones that depart more from equiprobability and are anti-correlated.

To demonstrate that these changes are indeed significant, Figs. 3.4(c,d) display the same probabilities, but calculated after the ISIs series have been shuffled (surrogate data). We can see that in these panels all the OPs and TPs are practically equiprobable, as expected, as no correlations exist in the surrogate data.

Comparing Fig. 3.3 with Figs. 3.4(a),(b) we see that at 7 MHz (when p_1 is maximum) and at 14 MHz (when $p_1 \sim p_2$) nothing remarkable occurs in the symbols' statistics; however, for

higher modulation frequencies, changes in the ISI distributions manifest also in changes in the statistics of the OP probabilities and transitions between OPs: the maximum of p_2 and p_3 (occurring at 26 MHz and at 39 MHz respectively) are located just after the local maxima (minima) of the $\mathrm{TP}_{01\to 01}$ (OP '210' probability), and the "equilibrium" situations ($p_2 \sim p_3$ at 31 MHz and $p_3 \sim p_4$ and 49 MHz) occur just after the local minima (maxima) of $\mathrm{TP}_{01\to 01}$ (OP '210' probability).

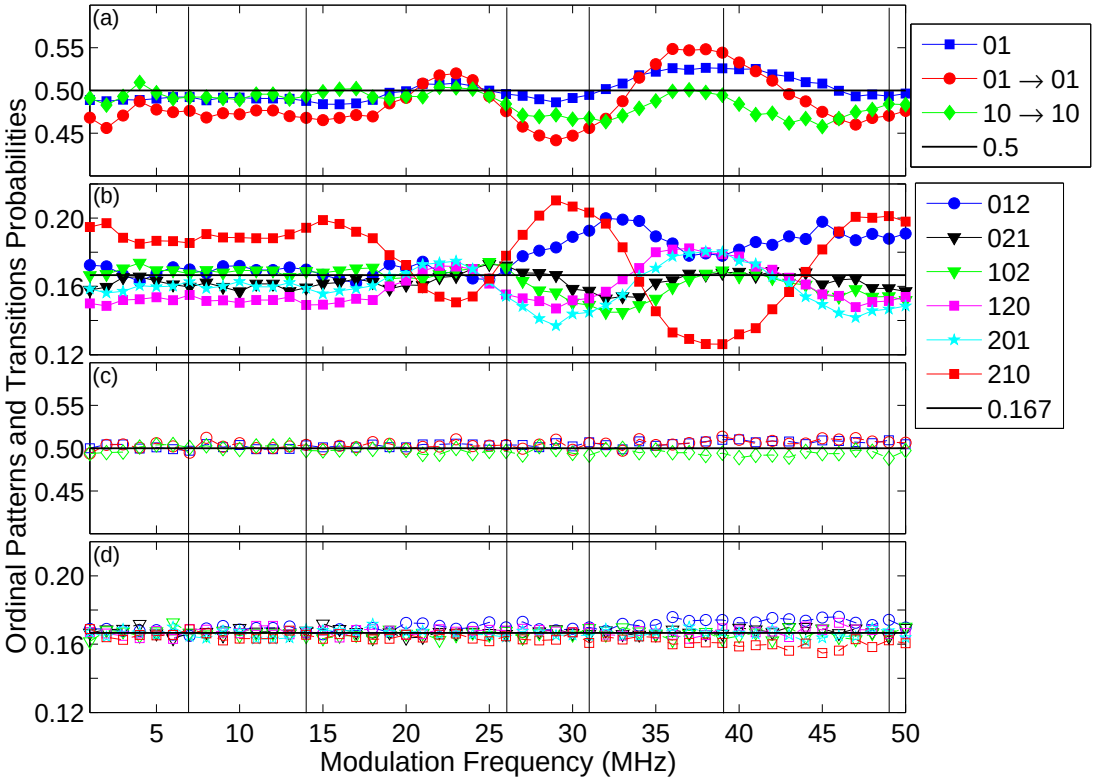

Figure 3.4: (a) Probabilities of $D = 2$ ordinal patterns and the transition probabilities. (b) $D = 3$ OPs probabilities. (c), (d) Same as (a),(b) but when the OPs and TPs are computed from surrogate (shuffled) IDI sequences.

To demonstrate that the above observations are robust, in Fig. 3.5 we plot the probabilities $p_0 \ldots p_4$, as well as the OPs and TPs, for $D = 2$, for weaker and for stronger modulation amplitudes. For the different amplitudes, above 20 MHz, the maxima and minima of the $\mathrm{TP}_{01\to 01}$ curve precede the maxima and the "equilibria" of the p_n probabilities. For strong amplitude we can see that, as p_4 (pink curve) vanishes (and therefore the "equilibrium point" between p_3 and p_4 also disappears), the local maximum and minimum in the transition probability curve also disappear. One remarkable feature is the structure that appears in the

TPs in the low frequencies (< 5 MHz) with the increasing amplitude. This structure does not appear to be linked with changes in the ISI distribution, at least for the wide bins (centered at nT_{mod}) used in this analysis. To check this hypothesis we used narrower bins and plotted all probability density functions for lower frequencies for all amplitudes but up to now the origin of this structure is unclear. We speculate that it could be related to $1:m$ phase-locking (m spikes per modulation cycle).

In the experiment we also used different external cavity lengths corresponding to feedback delays of 2.5, 7.5 and 10 ns. Qualitative similar behavior was observed, with similar structures also appearing in the lower frequencies for delays of 2.5 ns and 7.5 ns.

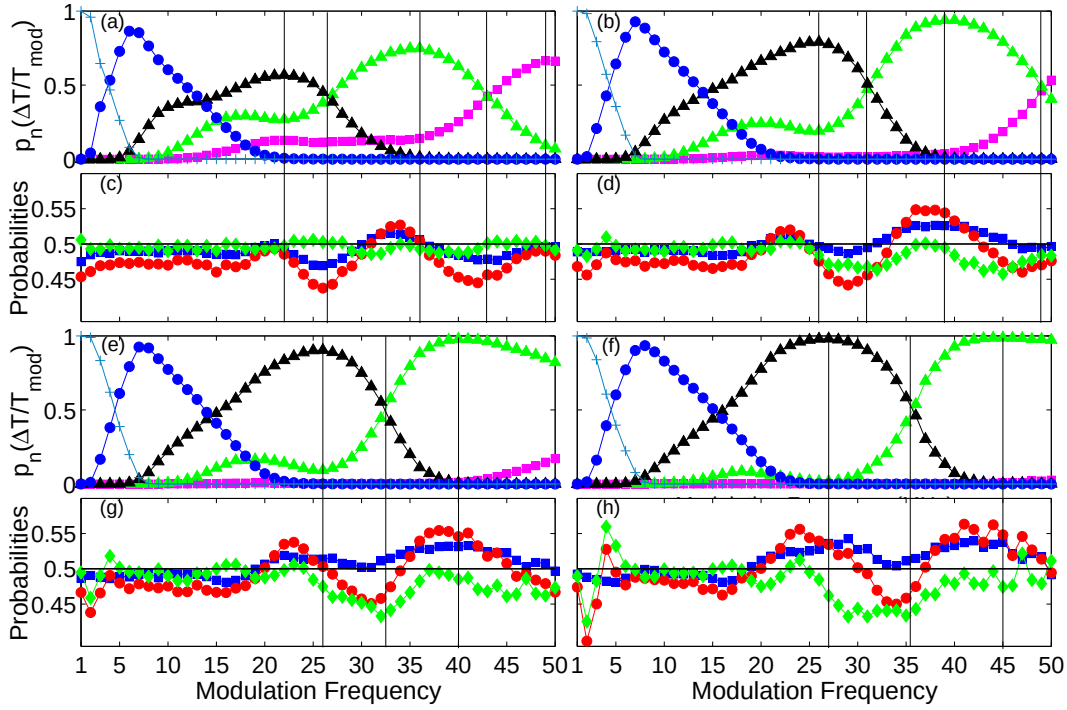

Figure 3.5: Histograms probabilities and OPs and transition probabilities for $D = 2$ versus modulation frequency for four different modulation amplitudes. 0.8% of I_{DC} (a,c); 1.2% (b,d); 1.6% (e,g); 2.0% (f,h). Legends as in Figs. 3.3 and 3.4(a).

3.3 Comparison with Lang and Kobayashi Simulations

Figure 3.6 shows a comparison between experimental and numerical OP and transition probabilities for the lower experimental modulation amplitude. The modulation amplitude is 0.8% of the DC current for the experimental data, panels 3.6(a) and 3.6(c). In the simulations,

panels 3.6(b) and 3.6(d), the modulation amplitude parameter is $a = 0.004$, corresponding to a peak-to-peak amplitude of 0.8% of μ_0, the DC current parameter. For the numerical data the probabilities change slower with the varying frequency than in the experimental data, but present the same general trends. As the model is a quite simple one (it takes into account only one reflection in the external cavity and neglects multi-mode emission, spatial and thermal effects) only a qualitative agreement could be expected. We find it remarkable that no re-scaling or major changes in the parameters of the model are needed to reproduce the general behavior of the probabilities. The agreement is not good for stronger modulation amplitude. More detailed numerical investigations are ongoing and should be reported elsewhere.

It is important to note that for $D = 3$ OPs, two clusters of OPs, formed by '021-102' and '120-201', where the OPs occur with the same probability, appear in the entire frequency range both for experimental and numerical data, being more clearly visible for higher frequencies. These clusters were reported in [97, 98] and were explained in terms of a simple model that was previously used to model temporal correlations in sensory neurons. Thus, we demonstrate here that the two clusters are robust and persist over a wide range of modulation frequencies.

3.4 Conclusions

We have experimentally investigated the spiking output of a semiconductor laser with optical feedback in the LFF regime, under weak current modulation. In this regime the laser behaves as a weakly forced excitable system. We focused on the effects of varying the modulation frequency in the sequence of inter-spike-intervals (ISIs). With increasing modulation frequency the ISIs become larger multiples of the modulation period. We found that the mean ISI does not decrease monotonically as the modulation frequency increases, but displays smooth oscillations and plateau-like behavior due to noisy phase-locking. By using a symbolic method of analysis capable of detecting temporal correlations in data sets, we identified subtle changes in the correlations present in the ISI sequence (revealed by variations in the probabilities of the ordinal patterns and transitions), that complement the information extracted from the ISI distribution. The smooth variations in the symbolic probabilities were shown to be related to changes seen in the ISI distribution. For increasing modulation amplitude we observed that the phase-locking regions migrate to higher frequencies, became

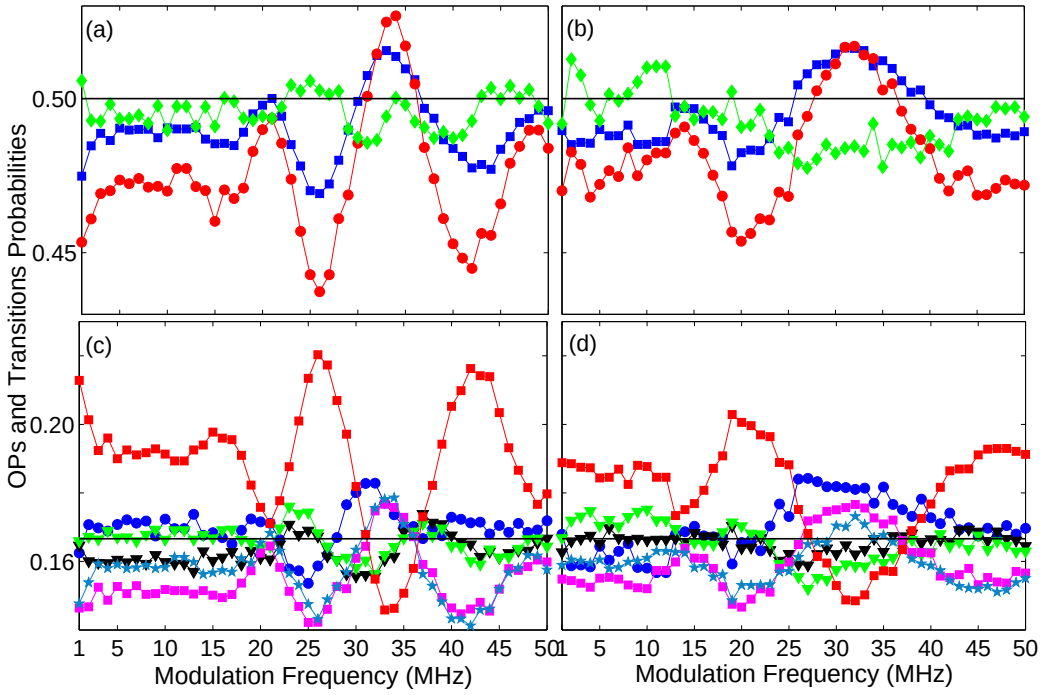

Figure 3.6: First row: OP and transition probabilities for $D = 2$. (a) Experimental, (b) Numerical. Second row: OP probabilities for $D = 3$. (c) Experimental, (d) Numerical. Modulation amplitude: 0.8% of I_{DC}. Legends as in Fig. 3.4.

wider and the locking became more clear. We have also shown that, for appropriated parameters, simulations of the Lang and Kobayashi model are in good qualitative agreement with the experimental results.

The symbolic methodology used is an efficient way to detect subtle changes in noisy correlated data sets and may be applied to investigate other optical excitable devices.

Chapter

4

Influence of the Natural Spike Rate on the Symbolic Dynamics of the Laser

In this chapter we investigate experimentally how changes in the external cavity length and DC current affect the mean inter-spike-interval (ISI) in a modulated semiconductor laser with optical feedback operating in the low-frequency fluctuations regime. The variation of the mean ISI with the modulation frequency is shown to be more pronounced when time delay and DC current allow for low spike rate. We use the method of ordinal symbolic analysis to examine how time correlations (among 3, 4 and 5 consecutive laser spikes) change with the spike rate. This method is able to capture subtle changes, otherwise hidden in the dynamics. We find that higher spike rates wash out the effects of the modulation in the time correlations. Simulations using the Lang and Kobayashi model are in good qualitative agreement with the experimental observations. The results in this chapter are going to be published in reference [102]. Experiments described here were performed in collaboration with Carlos Quintero-Quiroz.

4.1 Experimental Setup

The experimental setup is depicted in Fig. 4.1. A semiconductor laser (Sony SLD1137VS), with a solitary threshold current I_{th} =28.40 mA, temperature- and current-stabilized with an accuracy of 0.01 C and 0.01 mA, respectively, using a diode laser combi controller (Thorlabs ITC501), emitting at 650 nm, has part of its output power fed back to the laser cavity by a mirror. A 50/50 beamsplitter in the external cavity sends light to a photo-detector (Thorlabs

DET210) that is connected to a fast amplifier (FEMTO HSA-Y-2-40), a 1 GHz digital storage oscilloscope (Agilent Technologies Infiniium DSO9104A) and a radio frequency spectrum analyzer (Anritsu MS2651B). A neutral density filter in the external cavity allows to control the feedback power. The laser is operated at 17.00 C and, unless stated, the threshold reduction due to feedback is 7.3%. In the experiment we used three external cavity lengths, corresponding to feedback delay times, τ, of 2.5, 5 and 7.5 ns, and the DC current value was varied in the range between between $1.01I_{th}$ and $1.05I_{th}$.

A bias-tee in the laser mount allows the pump current to be modulated with a sinusoidal signal provided by a 80 MHz waveform generator (Agilent 33250A), with frequency varying from 1 to 50 MHz in steps of 1 MHz, and peak-to-peak amplitudes, A_{mod} = 0.8% and 1.6% of I_{th}. Only for the higher modulation amplitude and the lower I_{DC} the laser operates momentarily below the solitary threshold I_{th}, in a range where the LFFs are still observed, and no remarkable qualitative difference due to this fact appears. For all other values of modulation amplitude and I_{DC} the laser current is always above I_{th}. The experiment is controlled by a LabVIEW program that acquires the time series, detects the spikes, and calculates the inter-spike-intervals (ISIs) until a minimum of 60,000 ISIs are recorded. Then, the program changes the modulation frequency and/or amplitude, waits 10 seconds to let transients die away, and the process is repeated.

4.2 Analysis of the Spike Rate of the Modulated Laser

Time series showing the lasers spikes for different conditions are displayed in Fig. 4.2. In all the panels the time interval is 1 μs, and the modulation amplitude is 1.6% of I_{th}. The panels in the same line are for the same τ and I_{DC} (μ_0), the panels in the same column are for the same modulation frequency f_{mod}, or no modulation. In the panels 4.2a-c, where the parameters allow for a relatively slow LFF dynamics, we can see that a slow f_{mod} (4.2b) do not change remarkably the spike rate present in the unmodulated laser (4.2a), while a fast f_{mod} provokes a considerable increase in the spike rate as we can see in panel 4.2c, where the spikes are entrained: they occur each 3 or 4 modulation cycles. In the faster LFF dynamics of panels 4.2e-f we also see that the slow f_{mod} (4.2e) does not change much the spike rate we have in the unmodulated case (4.2d). In 4.2f the dropouts are also entrained, occurring each 2 or 3 modulation cycles.

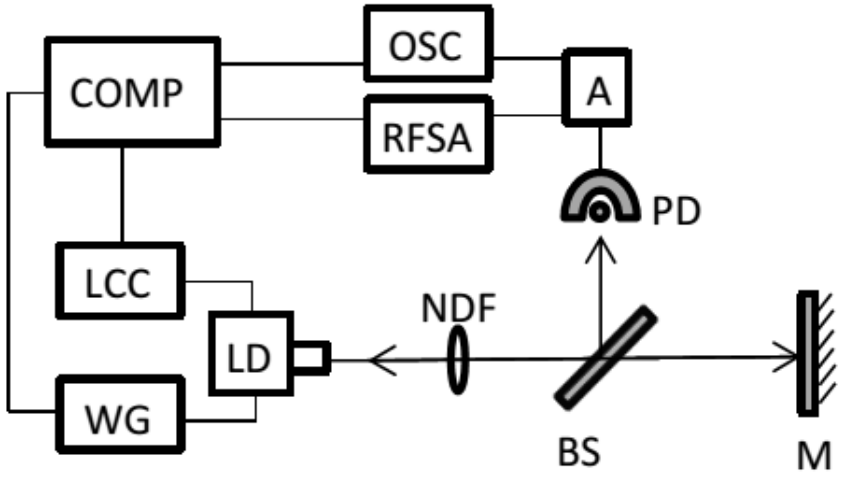

Figure 4.1: Schematics of the experimental setup. LD: laser diode; NDF: neutral density filter, BS: beam-splitter; M: mirror; PD: photo-detector; A: fast amplifier; OSC: digital storage oscilloscope; RFSA: radio frequency spectrum analyzer; COMP: computer; LCC: laser combi controller; WG: waveform generator.

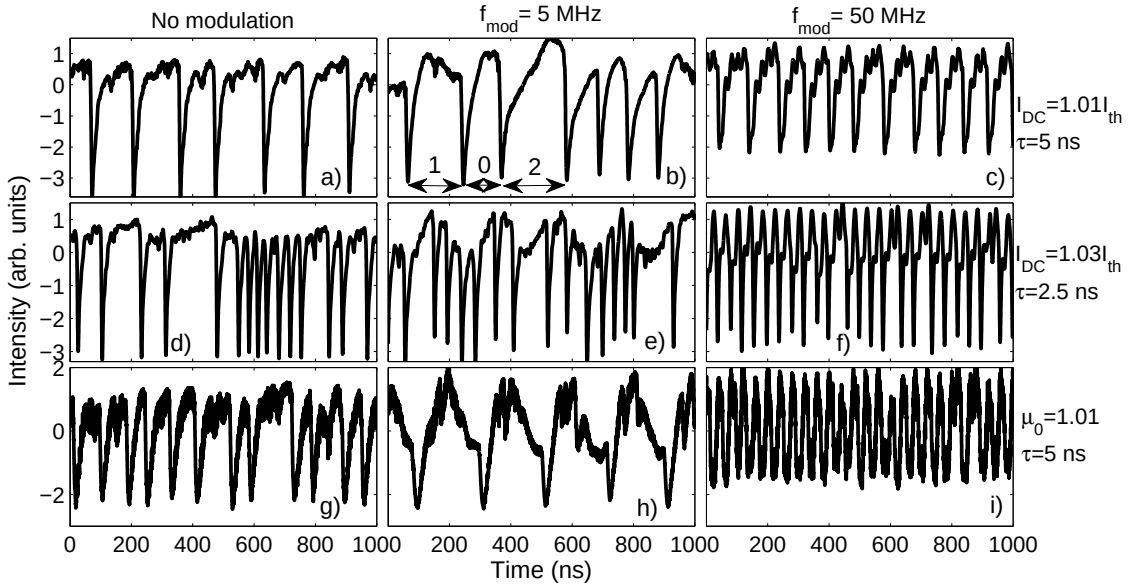

Figure 4.2: Experimental and simulated intensity time series with and without modulation for different spike rate conditions. A_{mod} = 1.6% of I_{th}. a-f: experimental. g-i: simulations. a-c: I_{DC}=1.01I_{th}, τ=5 ns. d-f: I_{DC}=1.03I_{th}, τ=2.5 ns. g-i: μ_0=1.01, τ=5 ns. a,d,g: no modulation. b,e,h: f_{mod}= 5 MHz. c,f,i: f_{mod}= 50 MHz.

Panels 4.2g-h display time series simulated with the Lang and Kobayashi model, for μ_0 = 1.01 and τ = 5 ns. The LFF dynamics is a bit faster in the simulations. Despite this fact, we

shall see that the influence of τ and I_{DC} in the spike rates and correlations observed in the experiments is qualitatively well reproduced by the model. We note a general qualitative agreement between panels 4.2a-c and 4.2g-i. For fast f_{mod}, the dropouts in the numerical series are also entrained, occurring each 2 or 3 modulation cycles (panel 4.2i).

The effects of varying the time delay and the pump current on the experimental spike rate are shown in Fig. 4.3. The modulation amplitude is as in Fig. 4.2. In panel 4.3a the mean ISI for three external cavities, corresponding to time delays of 2.5, 5 and 7.5 ns, are plotted against the modulation frequency. The curves for 5 and 7.5 ns present a plateau for low frequencies, followed by a rapid decrease in the mean ISIs as the modulation frequency increases, and a local minimum and maximum, after which the mean ISI varies little for 7.5 ns, and continue to decrease for 5 ns. The local minimum and maximum occur for higher frequencies in the curve for 5 ns and are absent in the curve for 2.5 ns, where the mean ISI decrease almost monotonically. Varying the current, in Fig. 4.3b, one can follow the variations in the spike rate in a more gradual way. In panel 4.3b the curves for low I_{DC} resemble the curves for $\tau = 5$, 7.5 ns in 4.3a. As the current increases, the plateau in the low frequency region increases and local minimum and maximum move to higher frequencies, while the curves become more flat.

Figure 4.4 presents the results of simulations. The mean ISI vs. modulation frequency for different τ and μ_0 is displayed. The numerical curves resemble the experimental ones, the plateau for low frequency and the following rapid decrease can be seen. The main difference is the oscillations that occur at intermediate and high frequencies, much stronger in the experimental curves. We can see a small oscillation in the curves for $\tau = 5$, 7.5 ns in panel 4.4a and the curve for $\mu_0 = 1.01$ in panel 4.4b.

From Figs. 4.3 and 4.4 we can conclude that when the parameters are such that the natural spike rate (without modulation) is slow (i.e., for long delay or low I_{DC}) then, the modulation frequency affects more strongly the mean ISI, that, with exception of a few narrow intervals, decreases with increasing modulation frequency. In other words, faster modulation is able to produce faster spikes. On the contrary, when the spikes without modulation are already fast (for short delay or for large I_{DC}) then, the modulation frequency has a smaller effect in the spike rate.

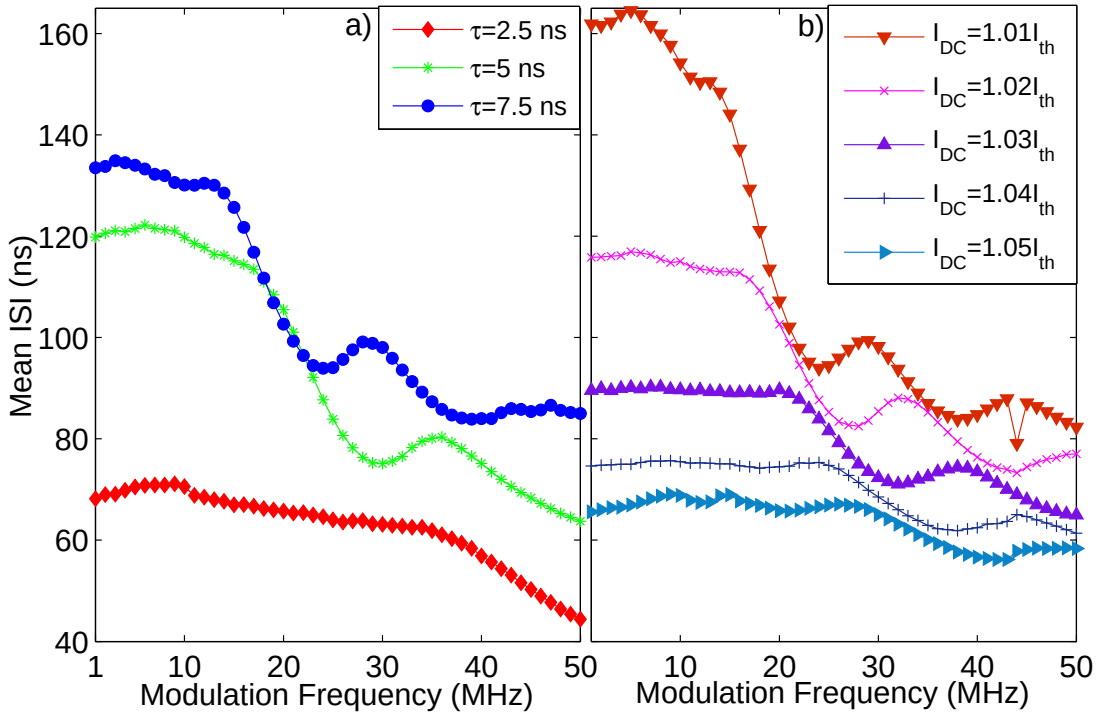

Figure 4.3: a) Experimental mean ISI as function of the modulation frequency for three different time delays. 2.5 and 7.5 ns: $I_{DC} = 1.03 I_{th}$. 5 ns: $I_{DC} = 1.024 I_{th}$, threshold reduction of 7.1%. b) Experimental mean ISI as function of the modulation frequency for five different DC currents. $\tau = 5$ ns. $A_{mod} = 1.6\%$ of I_{th}.

4.3 Analysis of Spike Correlations via Ordinal Symbolic Analysis

Although ordinal symbolic analysis does not take into account the exact duration of the inter-spike-intervals, it can capture subtle changes in time correlations among consecutive laser spikes, as the underlying correlations affect the probabilities of the ordinal patterns (OPs): if no correlations are present in the spike sequence, all OPs are equally probable; as there are $D!$ possible OPs of dimension D, their expected probability is $1/D!$. Thus, if there are OPs whose probability is significantly different from $1/D!$, they unveil the existence of serial correlations in the timing of the laser spikes.

Figure 4.5 displays the results of the analysis of the experimental data: the probability of the pattern '210' is plotted for three delays and two modulation amplitudes. By analyzing the probability of this pattern, we investigate the existence of time correlations among 4

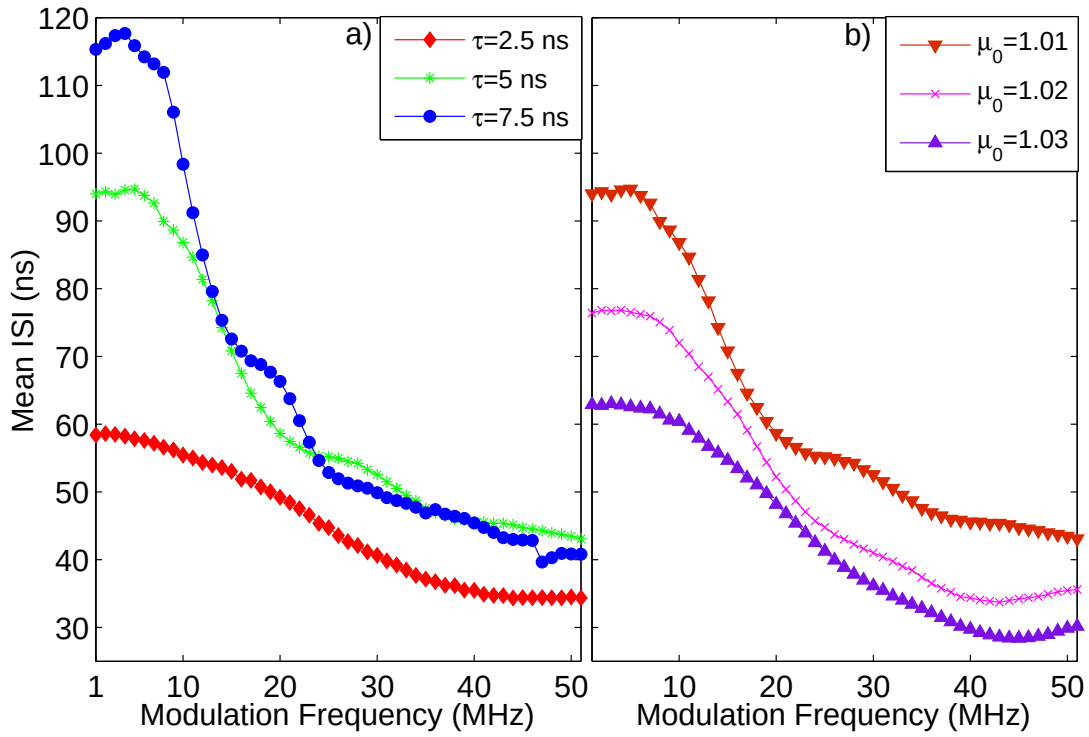

Figure 4.4: a) Mean ISI from simulations as function of the modulation frequency for three different time delays. $\mu_0 = 1.01$. b) Mean ISI from simulations as function of the modulation frequency for three different DC current parameters, μ_0. $\tau = 5$ ns. $A_{mod} = 1.6\%$.

consecutive spikes. We chose this pattern because its probability is the one that differs the most from the $1/6$ value expected if no correlations are present in the spike sequence (i.e., if all the patterns are equally probable). In order to demonstrate that the probability of this pattern indeed unveils the presence of spike correlations, in Fig. 4.5 we also plot in empty symbols the probability of '210' computed from surrogate data, i.e., when we shuffle the ISIs.

In panel 4.5a there is a clear oscillation in the probability for intermediate frequencies. Observation of the changes in this oscillation pattern along the two columns (different amplitudes) and the three lines (different time delays), leads to the following conclusions: i) the increase of the modulation amplitude increases the differences between maxima and minima and moves the oscillation pattern to higher frequencies; ii) the decrease in the time delay decreases the differences between maxima and minima and moves the oscillation pattern to higher frequencies, in such a way that for 2.5 ns delay we can see only the first local minimum of the oscillation pattern.

In Fig. 4.6 we present the analysis of simulated data: the probability of '210' for original

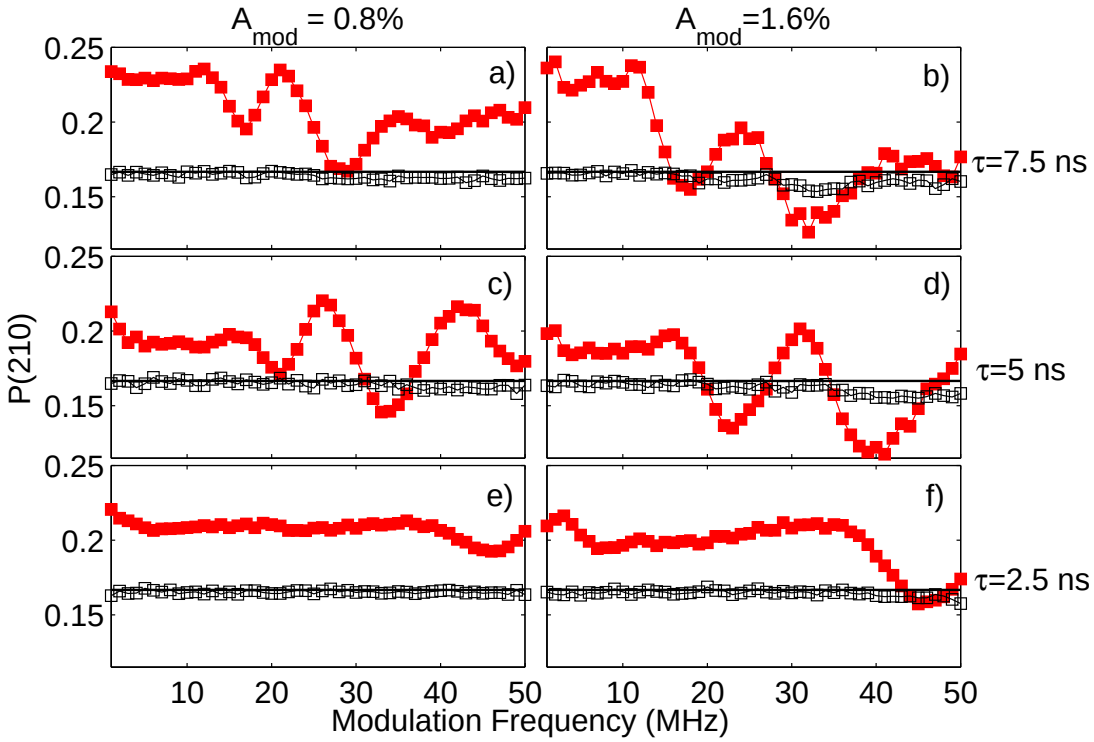

Figure 4.5: Symbolic analysis of experimental ISI data: '210' probability against modulation frequency, for two modulation amplitudes and three time delays. a-b: $\tau = 7.5$ ns, $I_{DC} = 1.03 I_{th}$. c-d: $\tau = 5$ ns, $I_{DC} = 1.024 I_{th}$, threshold reduction: 7.1%. e-f: $\tau = 2.5$ ns, $I_{DC} = 1.03 I_{th}$. a,c,e: $A_{mod} = 0.8\%$ of I_{th}. b,e,f: $A_{mod} = 1.6\%$ of I_{th}. Full symbols: original data. Empty symbols: surrogate data.

and surrogate data. A good agreement with the experimental results of Fig. 4.5 is observed.

A similar behavior is observed when the DC value of the injection current changes. In Fig. 4.7 we plot, for experimental ISIs, the probability of the '210' pattern for five different DC currents for the same modulation amplitudes and time delays as in Fig. 4.5. The variation of the oscillation pattern in the '210' probability when I_{DC} increases is the same as in Fig. 4.5 when τ decreases, as in both cases the intrinsic (without modulation) spike rate increases. For the higher amplitude (1.6%, second column) maxima and minima are more pronounced, and they occur at higher modulation frequencies. For increasing injection current (from top to bottom) the probability curve becomes more flat, as the oscillation pattern moves to higher frequencies. These observations are the same for Fig. 4.8, where the probabilities for the pattern '210' are plotted for the simulated ISIs, for the same values of μ_0 used in Fig. 4.4b.

From the observations above we can see that, as the dynamics becomes faster and the

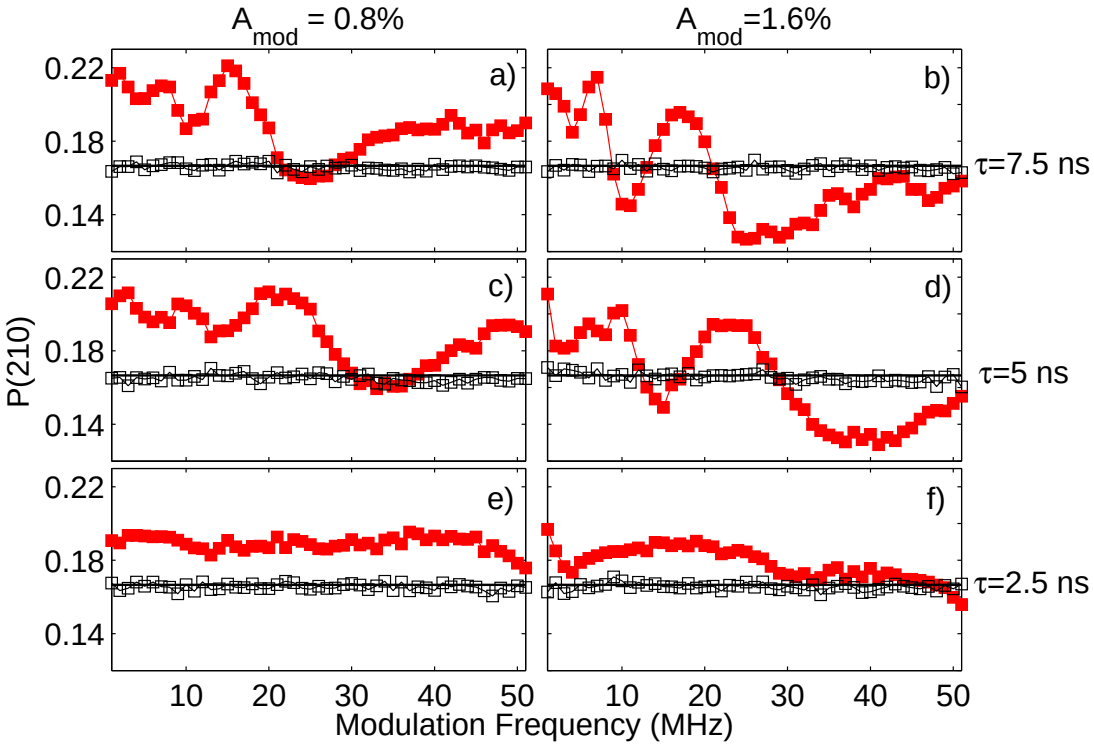

Figure 4.6: Symbolic analysis of simulated ISI data: '210' probability against modulation frequency, for two modulation amplitudes and three time delays. μ_0 = 1.01. a-b: τ= 7.5 ns. c-d: τ = 5 ns. e-f: τ = 2.5 ns. a,c,e: A_{mod} = 0.8% of I_{th}. b,e,f: A_{mod} = 1.6% of I_{th}. Full symbols: original data. Empty symbols: surrogate data.

spike rate increases, the differences in the time correlations among 4 consecutive spikes for the different modulation frequencies fade away. Figure 4.9, that displays for experimental data the probabilities of the '10' (top row) and the '3210' (bottom row) patterns vs. the modulation frequency and I_{DC}, shows that it also occurs for the correlations among 3 and among 5 consecutive spikes. The same general trends observed for '210' can be seen here as the maxima and minima move to higher frequencies (see the color patterns shifting to the right and to the top) and the differences between maxima and minima diminish, as the injection current increases.

These results demonstrate that serial spike correlations tend to diminish as the spike rate of the unmodulated laser becomes faster (the laser spike rate increases either when the delay time is decreased, or when the pump current is increased).

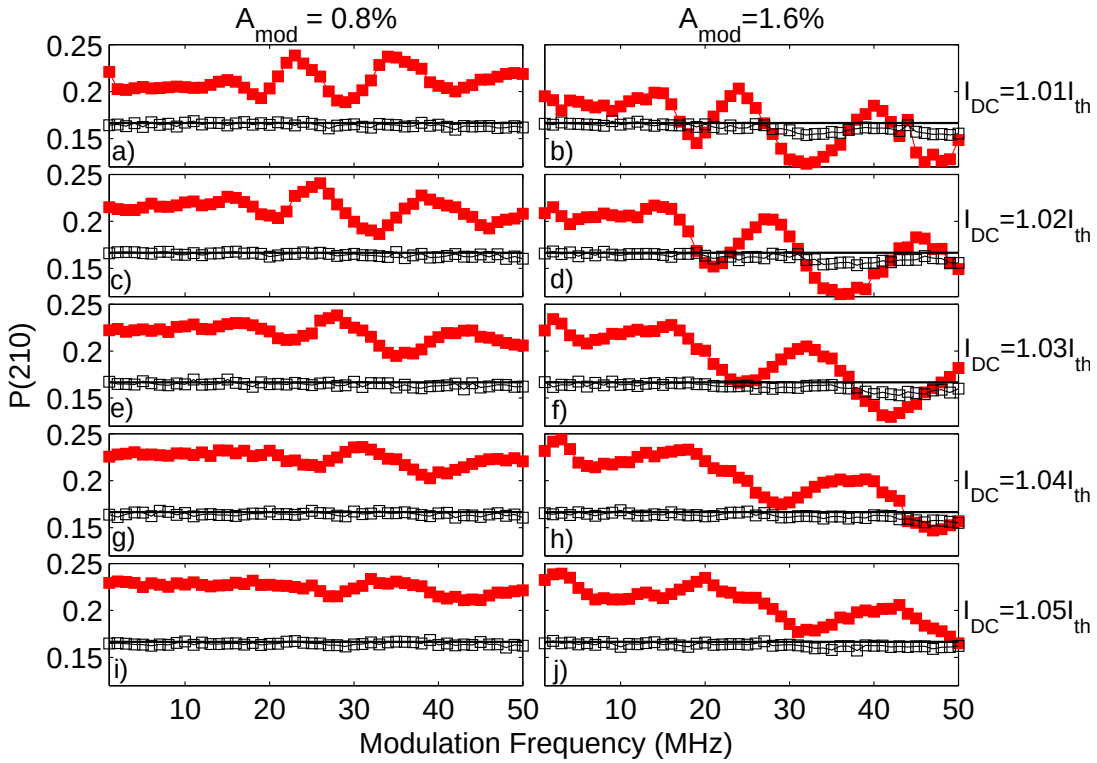

Figure 4.7: Symbolic analysis of experimental ISI data: '210' probability against modulation frequency, for two modulation amplitudes and five I_{DC}. $\tau = 5$ ns. a-b: $I_{DC} = 1.01I_{th}$. c-d: $I_{DC} = 1.02I_{th}$. e-f: $I_{DC} = 1.03I_{th}$. g-h: $I_{DC} = 1.04I_{th}$. i-j: $I_{DC} = 1.05I_{th}$. a,c,e,g,i: $A_{mod} = 0.8\%$ of I_{th}. b,d,f,h,j: $A_{mod} = 1.6\%$ of I_{th}. Full symbols: original data. Empty symbols: surrogate data.

4.4 Discussion

As we have seen, ordinal analysis provides information about the presence of underlying serial correlations in the spike sequence, which complements the information that can be gained by applying traditional time-series analysis tools. Many studies of the modulated LFFs, using return maps, spectral measurements, etc., have been reported in the literature. For example, by using return maps, Giudici *et al.* [65] and Sukow and Gauthier [99] demonstrated experimentally that spikes occur preferentially at time intervals that are multiples of the modulation period. Lam *et al.* [100] proposed an explanation based on the adiabatic motion of the ellipse formed by the steady state solutions of the Lang and Kobayashi model, due to slow modulation. On the other hand, Mendez *et al.* [103] showed that the organization of the experimental periodic orbits was equivalent to that of the periodic solutions of a

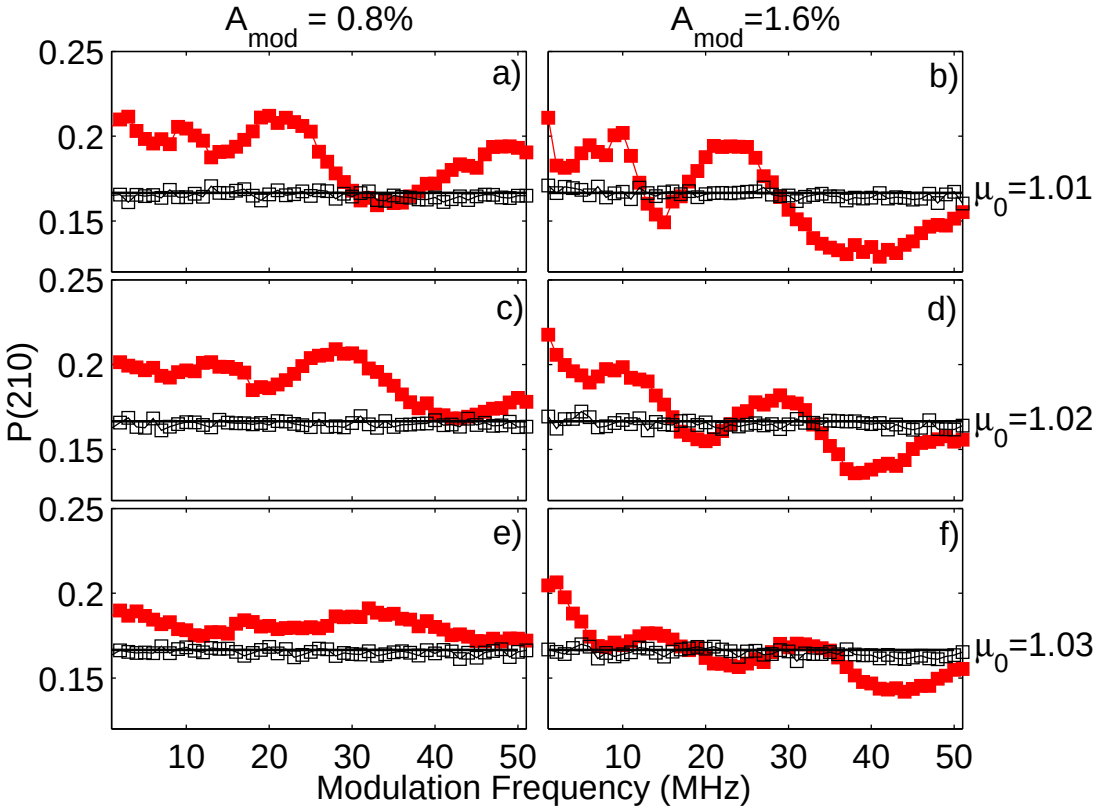

Figure 4.8: Symbolic analysis of simulated ISI data: '210' probability against modulation frequency, for two modulation amplitudes and three values of μ_0. τ = 5 ns. a-b: μ_0 = 1.01. c-d: μ_0 = 1.02. e-f: μ_0 = 1.03. a,c,e: A_{mod} = 0.8%. b,d,f: A_{mod} = 1.6%. Full symbols: original data. Empty symbols: surrogate data.

simple, low dimensional model proposed by Eguia *et al.* [90]. By analyzing the distribution of inter-spike-intervals, Buldú *et al.* [104] and Marino *et al.* [105] found evidence of stochastic resonance [106], as there is an optimal modulation frequency that maximizes the spike regularity.

In the previous chapter we used ordinal analysis to investigate how the correlations among several dropouts are affected by the modulation frequency and found that the minima and maxima of '210' OP probability were related to the noisy phase-locking of the spikes. Here we have focused on understanding how parameters that determine the natural spike rate (without modulation) affect this behavior. A crucial question remains that is: which physical mechanisms cause these correlations? While these are still unclear, because the same oscillations in the OP probabilities are seen in experimental and in numerical data, and they are clearly modified by model parameters (such as the pump current or the delay time), we

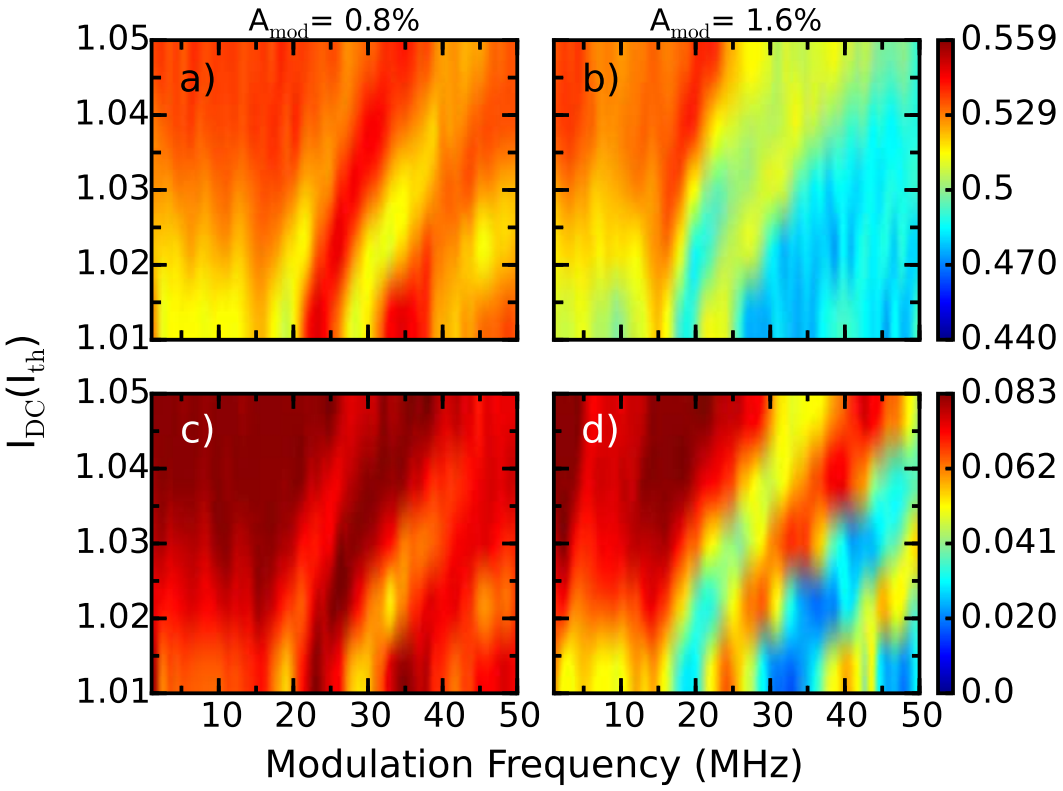

Figure 4.9: Symbolic analysis of experimental ISI data. a,b: '10' OP probability for varying I_{DC} and modulation current. c,d: '3210' OP probability for varying I_{DC} and modulation frequency. a,c: $A_{mod} = 0.8\%$ of I_{th}. b,d: $A_{mod} = 1.6\%$ of I_{th}.

speculate that the spike correlations are due to the specific organization of the trajectories in the system's phase space. The mechanisms responsible for spike correlations could also be related to the interplay of noise and modulation, in similar way as in stochastic resonance, where for an appropriated modulation frequency, the interplay of modulation and noise results in maximum spike regularity. Most importantly, these correlations could be generic features of periodically forced excitable systems: the observations of Feingold *et al.* [107] suggested that these systems can be described by circle maps, it was already shown [98] that a modified circle map adequately explains the correlations present in the LFF spikes, both, with and without modulation. In [98] it was shown that the OP probabilities (experimental observations and Lang and Kobayashi model simulations) display a well-defined, hierarchical and clustered structure, which is the same as that found in a modified circle map. Since the circle map describes many dynamical systems, including excitable ones, such correlations could also occur in other systems.

4.5 Conclusions

We have studied experimentally the dynamics of a directly modulated semiconductor laser with optical feedback in the LFF regime. Specifically, we studied how the external cavity length (i.e., the feedback delay time, τ) and the DC value of the injection current, I_{DC}, affect the mean inter-spike-interval (ISI) and the spike correlations.

Although increasing the modulation frequency in general tends to decrease the mean ISI, the effect is non-monotonous and there are some oscillations. Moreover, the modulation frequency can have a strong or a small effect in the spike rate, depending on the parameters. Specifically, if the laser spike rate, without modulation, is slow (for large τ or for low I_{DC}), increasing the modulation frequency results in considerably faster spikes; on the contrary, if the spike rate is fast (for short τ or for high I_{DC}), the modulation frequency has only a small effect on the spike rate, and fast modulation is unable to produce much faster spikes.

By using symbolic ordinal analysis we also studied how the changes in the spike rate affect the correlations among several consecutive spikes. We calculated the probabilities of occurrence of the ordinal patterns (OPs) that represent increasingly close spikes: '3210', '210' and '10'. We used a clearly visible oscillation pattern in the OPs' probability, when it is plotted against the modulation frequency, to track the changes in the temporal correlations. We found an equivalent effect when decreasing the time delay or when increasing the DC value of the injection current, as the pattern moves to higher modulation frequency and the differences between maxima and minima fade out. As the intrinsic spiking dynamics becomes faster, the effects of the current modulation become less pronounced and the temporal correlations for the different modulation frequencies become all alike.

We also analyzed simulated spike sequences, using the Lang and Kobayashi model with typical parameters, and found a good qualitative agreement with the experimental observations.

Our observations are important for developing optical neurons that fully mimic biological ones, which encode the information about external input signals in the spike rate and in the spike timing. In other words, neuronal systems use sequences of correlated spikes for information encoding and processing and therefore, spike correlations should be carefully taken into consideration when designing optical neurons that mimic the behavior of biological neurons. Our results suggest that there is limited range of modulation frequencies that

affect the spike rate and produce spike correlations: if the modulation is too fast, the spike correlations are washed out.

Chapter

5

Summary of Results and Future Work

5.1 Summary of Results

In this thesis we presented our findings after performing experimental and numerical investigations on the dynamics of the LFF regime in semiconductor lasers with optical feedback and current modulation. The study covers a comprehensive range of injection current, feedback delay time, modulation amplitude and modulation frequency.

The main method employed to perform the analysis was ordinal symbolic analysis, a nonlinear statistical tool that allows to unveil subtle serial correlations in time series. Experimental and numerical time series containing tens of thousands of LFF spikes were analyzed.

In Chapter 2 we used ordinal symbolic analysis to demonstrate the existence of a hierarchical, clustered organization of patterns in the excitable LFF regime which had not been previously noticed, despite all the attention that the LFF regime has attracted in the past decades. The cluster organization is robust to the presence of external forcing, implemented through current modulation. As the modulation amplitude is increased, a clear transition induced by the modulation was observed, as the patterns statistics reveal a highly stochastic behavior for no modulation and weak modulation and a deterministic behavior for high modulation amplitudes.

In Chapter 3 we focused on the effects of varying the modulation frequency in the sequence of ISIs. We found that with increasing modulation frequency the ISIs become larger multiples of the modulation period, but the mean ISI does not decrease monotonically, but displays smooth oscillations and plateau-like behavior due to noisy phase-locking. We found

that the smooth variations in the symbols probabilities are related to the changes in the shape of the ISIs distributions. If the modulation amplitude increases it becomes possible to have more effective phase-locking, which can occur at higher modulation frequencies. We also have shown that simulations of the LK model can reproduce qualitatively well the symbolic dynamics with varying modulation frequency.

In Chapter 4 we investigated how parameters that determine the natural (without modulation) spike rate affect both, the mean ISI and the spike correlations. We found that the modulation frequency can have a strong or a small effect in the spike rate, depending on the natural spike rate: if it is slow, increasing the modulation frequency results in considerably faster spikes; on the contrary, if the natural spike rate is fast, then, the modulation frequency has only a small effect on the spike rate, and fast modulation is unable to produce much faster spikes.

To investigate the changes in the temporal correlations we calculated the probabilities of occurrence of the ordinal patterns that represent increasingly close spikes: '3210', '210' and '10'. We found an equivalent effect when decreasing the time delay or when increasing the DC value of the injection current, as both parameters increase the natural spike rate. As the intrinsic spiking dynamics becomes faster, the effects of the modulation become less pronounced and the modulation frequency does not modify the temporal correlations.

We also analyzed simulated spike sequences, using the LK model with varying modulation frequency for different injection currents and feedback delay times, and found a good qualitative agreement with the experimental observations.

As biological neuronal systems use sequences of correlated spikes for information encoding and processing, we suggest that spike correlations should be carefully taken into consideration when designing optical neurons that mimic the behavior of biological neurons.

In the system studied here, a semiconductor laser with optical feedback in the LFF regime, our results suggest that there is limited range of external forcing frequencies that affect the spike rate and the spike correlations: if the external modulation is too fast, the spike correlations are washed out.

5.2 Perspectives for Future Work

The following issues are interesting for future work:

- Investigate the role of various noise sources in the spike correlations and in the symbolic dynamics, both experimentally (by adding a random signal in the injection current or by injecting incoherent light in the laser) and with the LK model, having in mind that this system is known to present phenomena like coherence and stochastic resonance [104, 105].

- The feedback strength is an important parameter for both the dynamics of the system and for the spike rate. Additional work studying the effects of this parameter on the spike correlations would be a natural continuation for the present work.

- Compare the results presented here with other measures of n:m phase locking, such phase synchronization [108]. For this we need to extract a phase from the laser intensity time series (via Hilbert transform) and compare with the phase of the modulation, or analyze the phase difference between consecutive spikes.

- Spikes of semiconductor lasers in the LFF regime and spikes of biological neurons have interesting similarities. Both are excitable, the distribution of ISIs under external forcing have a similar shape and their serial correlations can be described by a modified circle map, as presented in [98]. Those results suggest that optical neurons displaying temporal spike correlations similar to biological ones, could be built using semiconductor lasers. It would be very interesting to study the dynamics of small networks of coupled semiconductor lasers in the LFF regime and to compare with biological neuronal networks. In particular, it will be interesting to analyze how spike correlations that encode an external input signal spread in a small network of coupled lasers (i. e., how the information about the input signal is transmitted to other lasers). These investigations are being carried out by Carlos Quintero-Quiroz and J. Aparicio Reinoso.

Bibliography

[1] A. Einstein, "Zur quantentheorie der strahlung," *Physikalische Zeitschrift*, vol. 18, pp. 121–128, 1917.

[2] N. G. Basov and A. M. Prokhorov, "Application of molecular beams for the radiospectroscopic study of rotational molecular spectra," *Zh. Eksp. Teor. Fiz.*, vol. 27, no. 4, pp. 431–438, 1954.

[3] J. P. Gordon, H. J. Zeiger, and C. H. Townes, "Molecular microwave oscillator and new hyperfine structure in the microwave spectrum of nh_3," *Physical Review*, vol. 95, pp. 282–284, 1954.

[4] A. L. Schawlow and C. H. Townes, "Infrared and optical masers," *Physical Review*, vol. 112, p. 1940, 1958.

[5] T. Maiman, "Stimulated optical radiation in ruby," *Nature*, vol. 187, pp. 493–494, Aug. 1960.

[6] A. Javan, W. B. Bennett Jr., and D. R. Herriott, "Population inversion and continuous optical maser oscillation in a gas discharge containing a He-Ne mixture," *Physical Review Letters*, vol. 6, pp. 106–110, Feb. 1961.

[7] L. Johnson, G. D. Boyd, K. Nassau, and R. Soden, "Continuous operation of the $CaWO_4 : Nd'+$ optical maser," in *Proceedings of the IRE*, vol. 50, p. 213, 1962.

[8] D. F. Nelson and W. S. Boyle, "A continuously operating ruby optical maser," *Applied Optics*, vol. 1, no. 2, pp. 181–183, 1962.

[9] G. Boyd, R. J. Collins, S. P. S. Porto, A. Yariv, and W. A. Hargreaves, "Excitation, relaxation, and continuous maser action in the 2.613-micron transition of $CaF_2 : U^{3+}$," *Physical Review Letters*, vol. 8, pp. 269–272, Apr. 1962.

[10] N. G. Basov, O. N. Krokhin, and Y. M. Popov, "Production of negative temperature states in p-n junctions of degenerate semiconductors," *J. Exptl. Theoret. Phys. (U.S.S.R.)*, vol. 40, pp. 1879–1880, June 1961.

[11] N. R. Hall, G. E. Fenner, J. D. Kingsley, T. J. Soltys, and R. O. Carlson, "Coherent light emission from GaAs P-N junctions," *Physical Review Letters*, vol. 9, pp. 366–368, Nov. 1962.

[12] M. I. Nathan, W. P. Dumke, G. Burns, F. H. Dill, and G. Lasher, "Stimulated emission of radiation from GaAs P-N junctions," *Applied Physics Letters*, vol. 1, pp. 62–64, Nov. 1962.

[13] T. M. Quist, R. H. Rediker, R. J. Keyes, W. E. Krag, B. Lax, A. L. McWorther, and H. J. Zeiger, "Semiconductor maser of GaAs," *Applied Physics Letters*, vol. 1, pp. 91–92, Dec. 1962.

[14] N. Holonyak and S. F. Bevacqua, "Coherent (visible) light emission from $Ga(As_{1-x}P_x)$ junctions," *Applied Physics Letters*, vol. 1, pp. 81–83, Dec. 1962.

[15] H. Kroemer, "A proposed class of hetero-junction injection lasers," in *Proc. IEEE*, vol. 51, pp. 1782–1783, 1963.

[16] H. Kressel and H. Nelson, "Close-confinement gallium arsenide pn junction lasers with reduced optical loss at room temperature," *RCA Review*, vol. 30, pp. 106–113, Mar. 1969.

[17] I. Hayashi, M. B. Panish, and P. W. Foy, "A low-thresold room-temperature injection laser," *IEEE Journal of Quantum Electronics*, vol. QE-5, pp. 211–212, Apr. 1969.

[18] Z. I. Alferov, V. M. Andreev, E. L. Portnoi, and M. K. Trukan, "AlAs-GaAs heterojunction injection lasers with a low room-temperature threshold," *Soviet Physics-Semiconductors*, vol. 3, pp. 1107–1110, Mar. 1970.

[19] I. Hayashi, M. B. Panish, and P. W. Foy, "Junction lasers which operate continuously at room temperature," *Applied Physics Letters*, vol. 17, pp. 109–111, Aug. 1970.

[20] Z. Alferov, V. M. Andreev, E. L. Portnoi, and M. K. Trukan, "Investigation of the influence of the AlAs-GaAs heterostructure parameters on the laser threshold current and the realization of continuous emission at room temperature," *Soviet Physics-Semiconductors*, vol. 4, pp. 1573–1575, Mar. 1971.

[21] W. W. Chow and S. W. Koch, *Semiconductor-Laser Fundamentals*. Springer-Verlag, 1999.

[22] V. Gribkovskii, "Injection lasers," *Progress in Quantum Electronics*, vol. 19, no. 1, pp. 41–88, 1995.

[23] M. Yamada, *Theory of Semiconductor Lasers: From Basis of Quantum Electronics to Analyses of the Mode Competition Phenomena and Noise*. Springer Series in Optical Sciences, Springer, 2014.

[24] T. Numai, *Fundamentals of Semiconductor Lasers*. Springer Series in Optical Sciences, Springer-Verlag, 2004.

[25] N. Holonyak, R. Kolbas, R. D. Dupuis, and P. D. Dapkus, "Quantum-well heterostructure lasers," *IEEE Journal of Quantum Electronics*, vol. 16, pp. 170–186, 1980.

[26] Y. Arakawa and A. Yariv, "Quantum well lasers-gain, spectra, dynamics," *IEEE Journal of Quantum Electronics*, vol. 22, pp. 1887–1899, 1986.

[27] J. Buus, *Single Frequency Semiconductor Lasers*. SPIE Optical Engineering Press, 1991.

[28] J. Ohtsubo, *Semiconductor Lasers: Stability, Instability and Chaos*, vol. 111 of *Springer Series in Optical Sciences*. Springer, 2013.

[29] J. Tiana-Alsina, *Stochasticity, complexity and synchronization in semiconductor lasers*. PhD thesis, Universitat Politècnica de Catalunya, Terrassa, Spain, 2011.

[30] A. Aragoneses, *Experimental study of feedback-induced dynamics in semiconductor lasers: from symbolic analysis to subwavelength position sensing*. PhD thesis, Universitat Politècnica de Catalunya, Terrassa, Spain, 2014.

[31] C. H. Henry, "Theory of the linewidth of semiconductor lasers," *IEEE Journal of Quantum Electronics*, vol. 18, pp. 259–264, 1982.

[32] C. E. Wieman and L. Hollberg, "Using diode lasers for atomic physics," *Review of Scientific Instruments*, vol. 62, pp. 1–20, Jan. 1991.

[33] D. M. Kane and K. A. Shore, eds., *Unlocking Dynamical Diversity - Optical Feedback Effects on Semiconductor Lasers*. John Wiley and Sons, 2005.

[34] C. Ye, *Tunable External Cavity Diode Lasers*. World Scientific Publishing, 2004.

[35] S. Donati, "Developing self-mixing interferometry for instrumentation and measurements," *Laser & Photonics Reviews*, vol. 6, no. 3, pp. 393–417, 2012.

[36] S. Donati, G. Giuliani, and S. Merlo, "Laser diode feedback interferometer for measurement of displacements without ambiguity," *IEEE Journal of Quantum Electronics*, vol. 31, pp. 113–119, 1995.

[37] W. M. Wang, K. T. V. Grattan, A. W. Palmer, and W. J. O. Boyle, "Self-mixing interference inside a single-mode diode laser for optical sensing applications," *Journal of Lightwave Technology*, vol. 12, pp. 1577–1587, 1994.

[38] G. Giuliani and M. Norgia, "Laser diode linewidth measurement by means of self-mixing interferometry," *IEEE Photonics Technology Letters*, vol. 12, pp. 1028–1030, 2000.

[39] Y. Yu, G. Giuliani, and S. Donati, "Measurement of the linewidth enhancement factor of semiconductor lasers based on the optical feedback self–mixing effect," *IEEE Photononics Technology Letters*, vol. 16, pp. 990—992, 2004.

[40] F. T. Arecchi, G. L. Lippi, G. P. Puccioni, and J. R. Tredicce, "Deterministic chaos in laser with injected signal," *Optics Communications*, vol. 51, pp. 308–314, 1984.

[41] S. H. Strogatz, *Nonlinear dynamics and chaos*. Westview Press, 1994.

[42] M. Sciamanna and K. A. Shore, "Physics and applications of laser diode chaos," *Nature Photonics*, vol. 9, pp. 151–162, 2015.

[43] R. Tkach and A. Chraplyvy, "Regimes of feedback effects in 1.5−μm distributed feedback lasers," *Journal of Lightwave Technology*, vol. 4, pp. 1655–1661, 1986.

[44] K. Kikuchi and T. Okoshi, "Simple formula giving spectrum narrowing ratio of semiconductor laser output obtained by optical feedback," *Electronics Letters*, pp. 10–11, 1982.

[45] R. Tkach and A. Chraplyvy, "Line broadening and mode splitting due to weak feedback in single frequency 1.5 μm lasers," *Electronics Letters*, vol. 21, pp. 1081–1083, 1985.

[46] D. Lenstra, B. Verbeek, and A. den Boef, "Coherence collapse in single-mode semiconductor lasers due to optical feedback," *IEEE Journal of Quantum Electronics*, vol. 21, pp. 674–679, 1985.

[47] M. Fleming and A. Mooradian, "Fundamental line broadening of single-mode (gaal)as diode lasers," *Applied Physics Letters*, vol. 38, pp. 511–513, 1981.

[48] M. Fleming and A. Mooradian, "Spectral characteristics of external-cavity controlled semiconductor lasers," *IEEE Journal of Quantum Electronics*, vol. 17, pp. 44–59, 1981.

[49] O. Hirota and Y. Suematsu, "Noise properties of injection lasers due to reflected waves," *IEEE Journal of Quantum Electronics*, vol. 15, pp. 142–149, 1979.

[50] T. Heil, I. Fischer, W. Elsässer, and A. Gavrielides, "Dynamics of semiconductor lasers subject to delayed optical feedback: the short cavity regime," *Physical Review Letters*, vol. 87, p. 243901, 2001.

[51] N. Schunk and K. Petermann, "Stability analysis for laser diodes with short external cavities," *IEEE Photonic Technology Letters*, vol. 1, pp. 49–51, 1989.

[52] C. Masoller, "Effects of the external cavity length in the dynamics of a semiconductor laser with optical feedback," *Optics Communications*, vol. 128, pp. 363–376, 1996.

[53] P. Besnard, B. Meziane, and G. M. Stephan, "Feedback phenomena in a semiconductor laser induced by distant reflectors," *IEEE Journal of Quantum Electronics*, vol. 29, pp. 1271–1284, 1993.

[54] T. Heil, I. Fischer, and W. Elsässer, "Coexistence of low-frequency fluctuations and stable emission on a single high-gain mode in semiconductor lasers with external optical feedback," *Physical Review A*, vol. 58, pp. R2672–R2675, 1998.

[55] T. Heil, I. Fischer, W. Elsässer, J. Mulet, and C. R. Mirasso, "Statistical properties of low-frequency fluctuations during single-mode operation in distributed-feedback lasers: experiments and modeling," *Optics Letters*, vol. 24, pp. 1275–1277, 1999.

[56] C. Masoller, "Spatiotemporal dynamics in the coherence collapsed regime of semiconductor lasers with optical feedback," *Chaos: An Interdisciplinary Journal of Nonlinear Science*, vol. 7, pp. 455–462, 1997.

[57] J. Mork, B. Tromborg, and J. Mark, "Chaos in semiconductor lasers with optical feedback - theory and experiment," *IEEE Journal of Quantum Electronics*, vol. 28, pp. 93–108, 1992.

[58] V. Ahlers, U. Parlitz, and W. Lauterborn, "Hyperchaotic dynamics and synchronization of external-cavity semiconductor lasers," *Physical Review E*, vol. 58, pp. 7208–7213, 1998.

[59] I. Fischer, G. van Tartwijk, A. M. Levine, W. Els´asser, E. G´obel, and D. Lenstra, "Fast pulsing and chaotic itinerancy with a drift in the coherence collapse of semiconductor lasers," *Physical Review Letters*, vol. 76, pp. 220–223, 1996.

[60] A. M. Levine, G. H. M. van Tartwijk, D. Lenstra, and T. Erneux, "Diode lasers with optical feedback: Stability of the maximum gain mode," *Physical Review A*, pp. R3436–R3439, 1995.

[61] Y. Liu, P. Davis, and Y. Takiguchi, "Recovery process of low-frequency fluctuations in laser diodes with external optical feedback," *Physical Review E*, vol. 60, pp. 6595–6601, 1999.

[62] G. H. M. van Tartwijk, A. M. Levine, and D. Lenstra, "Sisyphus effect in semiconductor lasers with with optical feedback," *IEEE Journal of Selected Topics on Quantum Electronics*, vol. 1, p. 466, 1995.

[63] M. Fujiwara, K. Kubota, and R. Lang, "Low-frequency intensity fluctuation in laser diodes with external optical feedback," *Applied Physics Letters*, vol. 38, pp. 217–220, 1981.

[64] Y. Hong and K. A. Shore, "Statistical measures of the power dropout ratio in semiconductor lasers subject to optical feedback," *Optics Letters*, vol. 30, pp. 3332–3334, 2005.

[65] M. Giudici, C. Green, G. Giacomelli, U. Nespolo, and J. R. Tredicce, "Andronov bifurcation and excitability in semiconductor lasers with optical feedback," *Physical Review E*, vol. 55, pp. 6414–6418, 1997.

[66] J. Mulet and C. R. Mirasso, "Numerical statistics of power dropouts based on the lang-kobayashi model," *Physical Review E*, vol. 59, pp. 5400–5405, 1999.

[67] J. M. Méndez, J. Aliaga, and G. B. Mindlin, "Limits on the excitable behavior of a semiconductor laser with optical feedback," *Physical Review E*, vol. 71, p. 026231, 2005.

[68] J. Murray, *Mathematical Biology*. Berlin–Heidelberg–New York: Springer, 1993.

[69] B. Lindner, J. García-Ojalvo, A. Neiman, and L. Schimansky-Geier, "Effects of noise in excitable systems," *Physics Reports*, vol. 392, pp. 321–424, 2004.

[70] T. Sano, "Antimode dynamics and chaotic itinerancy in the coherence collapse of semiconductor lasers with optical feedback," *Physical Review A*, vol. 50, pp. 2719—-2726, 1994.

[71] A. Torcini, S. Barland, G. Giacomelli, and F. Marin, "Low-frequency fluctuations in vertical cavity lasers: Experiments versus lang-kobayashi dynamics," *Physical Review A*, p. 063801, 2006.

[72] J. Zamora-Munt, C. Masoller, and J. García-Ojalvo, "Transient low-frequency fluctuations in semiconductor lasers with optical feedback," *Physical Review A*, vol. 81, p. 033820, 2010.

[73] D. Brunner, X. Porte, M. C. Soriano, and I. Fischer, "Real-time frequency dynamics and high-resolution spectra of a semiconductor laser with delayed feedback," *Scientific Reports*, vol. 2, p. 732, 2012.

[74] J. Hadamard, "Les surfaces à courbures opposées et leur lignes geodesiques," *Journal de Mathématiques Pures et Appliqués*, vol. 4, pp. 27–73, 1898.

[75] M. Morse, "Recurrent geodesics on a surface of negative curvature," *Transactions, American Mathematical Society*, vol. 22, pp. 84–100, 1921.

[76] M. Morse and H. Hedlund, "Symbolic dynamics," *American Journal of Mathematics*, vol. 60, pp. 815–866, 1938.

[77] C. S. Daw, C. E. A. Finney, and E. R. Tracy, "A review of symbolic analysis of experimental data," *Review of Scientific Instruments*, vol. 73, no. 2, pp. 915–930, 2003.

[78] J. M. Amigó, *Permutation Complexity in Dynamical Systems: Ordinal Patterns, Permutation Entropy and All That.* Springer, 2010.

[79] C. S. Daw, M. B. Kennel, C. E. A. Finney, and F. T. Connolly, "Observing and modeling nonlinear dynamics in an internal combustion engine," *Physics Letters E*, vol. 57, p. 2811, 1998.

[80] U. Schwarz, A. O. Benz, J. Kurths, and A. Witt, "Analysis of solar spike events by means of symbolic dynamics methods," *Astronomy and Astrophysics*, vol. 277, p. 215, 1993.

[81] C. Bandt and B. Pompe, "Permutation entropy: A natural complexity measure for time series," *Physical Review Letters*, vol. 88, p. 174102, 2002.

[82] C. E. Shannon, "A mathematical theory of communiaction," *The Bell System Technical Journal*, vol. 27, pp. 379–423, 1948.

[83] M. Zanin, L. Zunino, O. A. Rosso, and D. Papo, "Permutation entropy and its main biomedical and econophysics applications: A review," *Entropy*, vol. 14, pp. 1553–1577, 2012.

[84] E. P. J. S. Topics, "Recent progress in symbolic dynamics and permutation complexity. ten years of permutation entropy," vol. 222, June 2013.

[85] C. Masoller, Y. Hong, S. Ayad, F. Gustave, S. Barland, A. J. Pons, S. Gómez, and A. Arenas, "Quantifying sudden changes in dynamical systems using symbolic networks," *New Journal of Physics*, vol. 17, p. 023068, 2015.

[86] U. Parlitz, S. Berg, S. Luther, A. Schirdewan, J. Kurths, and N. Wessel, "Classifying cardiac biosignals using ordinal pattern statistics and symbolic dynamics," *Computers in Biology and Medicine*, vol. 42, pp. 319–327, 2012.

[87] J. Tiana-Alsina, M. C. Torrent, O. A. Rosso, C. Masoller, and J. García-Ojalvo, "Quantifying the statistical complexity of low-frequency fluctuations in semiconductor lasers with optical feedback," *Physical Review A*, vol. 82, p. 013189, 2010.

[88] M. Martin, A. Plastino, and O. Rosso, "Generalized statistical complexity measures: Geometrical and analytical properties," *Physica A*, vol. 369, pp. 439–462, 2006.

[89] N. Rubido, J. Tiana-Alsina, M. C. Torrent, J. García-Ojalvo, and C. Masoller, "Language organization and temporal correlations in the spiking activity of an excitable laser: Experiments and model comparison," *Physical Review E*, vol. 84, p. 026202, 2011.

[90] M. C. Eguia, G. B. Mindlin, and M. Giudici, "Low-frequency fluctuations in semiconductor lasers with optical feedback are induced with noise," *Physical Review E*, vol. 58, pp. 2636–2639, 1998.

[91] M. C. Soriano, L. Zunino, O. A. Rosso, I. Fischer, and C. R. Mirasso, "Time scales of a chaotic semiconductor laser with optical feedback under the lens of a permutation information analysis," *IEEE Journal of Quantum Electronics*, vol. 47, pp. 252–261, 2011.

[92] L. Zunino, M. C. Soriano, and O. A. Rosso, "Characterizing the hyperchaotic dynamics of a semiconductor laser subject to optical feedback via permutation entropy," *IEEE Jorunal of Selected Topics in Quantum Electronics*, vol. 17, pp. 1250–1257, 2011.

[93] S. Y. Xiang, W. Pan, L. S. Yan, B. Luo, X. H. Zou, N. Jiang, and K. H. Wen, "Quantifying chaotic unpredictability of vertical-cavity surface-emitting lasers with polarized optical feedback via permutation entropy," *IEEE Journal of Quantum Electronics*, vol. 17, pp. 1212–1219, 2011.

[94] J. P. Toomey and D. M. Kane, "Mapping the dynamic complexity of a semiconductor laser with optical feedback using permutation entropy," *Optics Express*, vol. 22, p. 1713, 2014.

[95] J. P. Toomey, D. M. Kane, and T. Ackemann, "Complexity in pulsed nonlinear laser systems interrogated by permutation entropy," *Optics Express*, vol. 22, pp. 17840–17853, 2014.

[96] B. Fadlallah, B. Chen, A. Keil, and J. Príncipe, "Weighted-permutation entropy: A complexity measure for time series incorporating amplitude information," *Physical Review E*, vol. 87, p. 022911, 2013.

[97] A. Aragoneses, T. Sorrentino, S. Perrone, D. J. Gauthier, M. C. Torrent, and C. Masoller, "Experimental and numerical study of the symbolic dynamics of a modulated external-cavity semiconductor laser," *Optics Express*, vol. 22, pp. 4705–4713, 2014.

[98] A. Aragoneses, S. Perrone, T. Sorrentino, M. C. Torrent, and C. Masoller, "Unveiling the complex organization of recurrent patterns in spiking dynamical systems," *Scientific Reports*, vol. 4, p. 4696, 2014.

[99] D. W. Sukow and D. J. Gauthier, "Entraining power-dropout events in an external-cavity semiconductor laser using weak modulation of the injection current," *IEEE Journal of Quantum Electronics*, vol. 36, pp. 175–183, 2000.

[100] W.-S. Lam, N. Parvez, and R. Roy, "Effect of spontaneous emission noise and modulation on semiconductor lasers near threshold with optical feedback," *International Journal of Modern Physics B*, vol. 17, pp. 4123—-4138, 2003.

[101] T. Sorrentino, C. Quintero-Quiroz, A. Aragoneses, M. C. Torrent, and C. Masoller, "Effects of periodic forcing on the temporally correlated spikes of a semiconductor laser with feedback," *Optics Express*, vol. 23, pp. 5571–5581, 2015.

[102] T. Sorrentino, C. Quintero-Quiroz, M. C. Torrent, and C. Masoller, "Analysis of the spike rate and spike correlations in modulated semiconductor lasers with optical feedback," *IEEE Journal of Selected Topics in Quantum Electronics*, 2015. in press.

[103] J. M. Mendez, R. Laje, M. Giudici, J. Aliaga, and G. B. Mindlin, "Dynamics of periodically forced semiconductor laser with optical feedback," *Physical Review E*, vol. 63, p. 066218, 2001.

[104] J. M. Buldú, J. García-Ojalvo, C. R. Mirasso, and M. C. Torrent, "Stochastic entrainment of optical power dropouts," *Physical Review E*, vol. 66, p. 021106, 2002.

[105] F. Marino, M. Giudici, S. Barland, and S. Balle, "Experimental evidence of stochastic resonance in an excitable optical system," *Physical Review Letters*, vol. 88, p. 040601, 2002.

[106] L. Gammaitoni, P. Hänggi, P. Jung, and F. Marchesoni, "Stochastic resonance," *Reviews of Modern Physics*, vol. 70, pp. 223–287, 1998.

[107] M. Feingold, D. L. Gonzalez, O. Piro, and H. Viturro, "Phase locking, period doubling, and chaotic phenomena in externally driven excitable systems," *Physical Review A*, vol. 37, pp. 4060–4063, 1988.

[108] P. Tass, M. G. Rosenblum, J. Weule, J. Kurths, A. Pikovsky, J. Volkmann, A. Schnitzler, and H. J. Freund, "Detection of n:m phase locking from noisy data: Application to magnetoencephalography," *Physical Review Letters*, vol. 81, pp. 3291–3294, 1998.

Publications

Articles in indexed journals and conference proceedings related to the work presented in this thesis:

- A. Aragoneses, T. Sorrentino, S. Perrone, D. J. Gauthier, M. C. Torrent, and C. Masoller. "Experimental and numerical study of the symbolic dynamics of a modulated external-cavity semiconductor laser." *Optics Express*, vol. 22, pp. 4705–4714, 2014.

- A. Aragoneses, S. Perrone, T. Sorrentino, M. C. Torrent, and C. Masoller. "Unveiling the complex organization of recurrent patterns in spiking dynamical systems." *Scientific Reports*, vol. 4, 4696, 2014.

- T. Sorrentino, A. Aragoneses, S. Perrone, D. J. Gauthier, M. C. Torrent, and Cristina Masoller. "Experimental study of the complex dynamics of semiconductor lasers with feedback via symbolic time-series analysis." *Proc. SPIE 9134, Semiconductor Lasers and Laser Dynamics VI*, 91340L. May 2, 2015. doi:10.1117/12.2052322

- T. Sorrentino, C. Quintero-Quiroz, A. Aragoneses, M. C. Torrent, and Cristina Masoller. "Effects of periodic forcing on the temporally correlated spikes of a semiconductor laser with feedback." *Optics Express*, vol. 23, pp. 5571–5581, 2015.

- T. Sorrentino, C. Quintero-Quiroz, M. C. Torrent, and C. Masoller. "Analysis of the Spike Rate and Spike Correlations in Modulated Semiconductor Lasers with Optical Feedback." *IEEE Journal of Selected Topics in Quantum Electronics*, in press, 2015.

Additional work not related to this thesis:

- C. Masoller, T. Sorrentino, M. Chevrollier and M. Oriá. "Bistability in Semiconductor Lasers With Polarization-Rotated Frequency-Dependent Optical Feedback." *IEEE Journal of Quantum Electronics*, vol. 43, pp. 261–268, 2007.

- C. Masoller, T. Sorrentino, M. Chevrollier and M. Oriá. "Semiconductor lasers under orthogonal frequency-dependent optical feedback: experiments and theory." *Lasers and Electro-Optics, 2007 and the International Quantum Electronics Conference. CLEOE-IQEC 2007. European Conference on*, 17-22 June 2007, Munich, German. doi: 10.1109/CLEOE-IQEC.2007.4386974

- M. Oriá, B. Farias, T. Sorrentino, and M. Chevrollier. "Multistability in the emission frequency of a semiconductor laser." *Journal of the Optical Society of America B*, vol. 24, pp. 1867–1873, 2007.

- L. B. Barbosa, T. Sorrentino, D. N. Ferreira, D. Reyes Ardila, M. Chevrollier, and M. Oriá. "Semiconductor laser with extended cavity and intracavity atomic filter." *Optics Letters*, vol. 32, pp. 1869–1871, 2007.

- T. Sorrentino, O. Di Lorenzo, L. C. de Oliveira, M. Chevrollier, and M. Oriá. "All-optical frequency-controlled frequency switch." *Journal of the Optical Society of America B*, vol. 27, pp. 1458–1463, 2010.

- T. Sorrentino, C. Masoller, C. Soares, I. Vidal, M. Oriá. "Diode laser operation under orthogonal feedback: Experiments and theory." IEEE Conference Proceedings,*Laser Dynamics and Nonlinear Photonics, 2011 Fifth Rio De La Plata Workshop on*, 6–9 Dec. 2011. doi:10.1109/LDNP.2011.6162068

Conference and Workshop Presentations

- V Rio de la Plata Workshop on Laser Dynamics and Nonlinear Photonics. *Orthogonal feedback induced frequency shift in diode lasers: experiments and theory*. Taciano Sorrentino, C. Masoller and M. Oriá. Colonia del Sacramento, Uruguay, 6–9 December, 2011. [Poster contribution]

- XXXV Brazilian Meeting on Condensed Matter Physics. *Characterizing the spiking activity of semiconductor lasers with current modulation and optical feedback via ordinal time-series analysis*. Taciano Sorrentino, Andrés Aragoneses, Nicolás Rubido, M. C. Torrent, Daniel J. Gauthier, Cristina Masoller. Águas de Lindóia, Brazil, 14–18 May, 2012. [Poster contribution]

- XXXV Brazilian Meeting on Condensed Matter Physics. *Symbolic statistical ordinal analysis distinguishes determinism from stochasticity in the spiking activity of semiconductor lasers with optical feedback*. Andrés Aragoneses, Nicolás Rubido, Taciano Sorrentino, M. C. Torrent, and Cristina Masoller. Águas de Lindóia, Brazil, 14–18 May, 2012. [Poster contribution]

- SPIE Photonics Europe 2014. *Experimental study of the complex dynamics of semiconductor lasers with feedback via symbolic time-series analysis*. Taciano Sorrentino, Andrés Aragoneses, Sandro Perrone, Daniel J. Gauthier, M. C. Torrent, and Cristina Masoller. Brussels, Belgium, 14–17 April, 2014. [Oral contribution]

- NOLINEAL 2014. *Symbolic dynamics of directly modulated semiconductor lasers with optical feedback*. Taciano Sorrentino, Andrés Aragoneses, Sandro Perrone, Daniel J.

Gauthier, M. C. Torrent, and Cristina Masoller. Badajoz, Spain, 4–6 June, 2014. [Oral contribution]

- III Jornada complexitat.cat (Catalan Network for the Study of Complex Systems). *Symbolic dynamics of directly modulated semiconductor lasers with optical feedback*. Taciano Sorrentino, Andrés Aragoneses, Sandro Perrone, Daniel J. Gauthier, M. C. Torrent, and Cristina Masoller. Barcelona, Spain, 9 June, 2014. [Poster contribution]

- 10th AIMS International Conference on Dynamical Systems, Differential Equations and Applications. *Ordinal time-series analysis applied to the characterization of a forced excitable system*. Taciano Sorrentino, Andrés Aragoneses, M. C. Torrent and Cristina Masoller. Madrid, Spain, 7–11 July, 2014. [Invited oral contribution]

Attendance to Courses, Schools and Research Stays

- Research stay of three months at the Laboratório de Física Atômica e Lasers, Departamento de Física, Universidade Federal da Paraíba, João Pessoa, PB, Brazil. 1 October - 31 December, 2011.
- International Centre for Theoretical Physics - South American Institute for Fundamental Research. **School on Nonlinear Optics and Nanophotonics**. IFT-UNESP, São Paulo, Brazil. 25 November - 6 December, 2013.
- National Instruments. **Curso de LABVIEW *Core 1***. Universitat Politècnica de Catalunya, Vinanova i la Geltrú, Spain. 17–19 March, 2014.
- Optical Society of America. **Siegman International School on Lasers 2014**. Stanford University, Stanford, California, USA. 3–8 August, 2014.